STING agonists drive recruitment and intrinsic type I interferon responses in monocytic lineage cells for optimal anti-tumor immunity[1]

Authors: Melanie Girard*‡, Tianning Yu*‡, Nathalia V Batista*, Karen K. M. Yeung*, Sara Lamorte†, Wenting Gao*, Miaoxi Liu*2, Tracy L. McGaha*,†, and Tania H. Watts*3

Affiliations:

* Department of Immunology, University of Toronto, Toronto, Canada.

†Tumor Immunotherapy Program, Princess Margaret Cancer Centre, University Health Network, Toronto, Canada.

‡Co-first authors.

Corresponding author: Dr. Tania H. Watts, Department of Immunology, University of Toronto, 1 King's College Circle, Toronto, ON M5S 1A8, Canada. E-mail address: tania.watts@utoronto.ca

Tel 416-978-4551

Running title: Monocytes lineage cells in STING agonist therapy

Abstract

The cyclic GMP-AMP synthase-stimulator of interferon genes (cGAS-STING) pathway, a sensor of cytosolic DNA, orchestrates the production of pro-inflammatory cytokines, chemokines, and type I interferons (IFN-I), thereby contributing to spontaneous tumor surveillance. Intratumoral delivery of synthetic STING agonists induces IFN-I dependent tumor regression in preclinical cancer models and is being tested clinically. In this study, we investigate the role of monocytic lineage (MCs) cells in response to STING agonist induced IFN-I signaling. We show that CCR2-deficient mice, lacking inflammatory MCs in the periphery, or Lyz2-Cre-IFNAR1$^{fl/fl}$ mice in which IFN-I signaling in monocytes is reduced, exhibit impaired responses to STING agonist therapy of MC38 and/or B16F10 tumors. STING agonist treatment induced CCR5-dependent migration of MCs carrying tumor antigen from the tumor to the lymph nodes. Single-cell RNA sequencing of CD45^{+} cells from lymph nodes and tumors of mice in which half the hematopoietic cells lack the interferon alpha/beta receptor 1 (IFNAR1) revealed that STING agonist therapy induces intrinsic IFNAR1-dependent acquisition of an inflammatory monocytic cell phenotype distinct from inflammatory cDC and a reduction in macrophages with a pro-tumor TGFβ/angiogenesis transcriptome. IL-18 - IL-18R1 interaction was the top predicted interaction between monocytic lineage cells and CD8^{+} T cells or NK cells. Blocking IL-18 reduced the therapeutic efficacy of STING agonist treatment in CCR2$^{+/+}$ but not CCR2$^{-/-}$ mice, implicating IL-18 production by the monocytes in STING agonist therapy of melanoma. These findings support a pivotal role for IL-18 producing inflammatory monocytic lineage cells in tumor control following STING agonist treatment.

46 **Introduction**

47 Monocytic lineage cells (MC), including monocytes, monocyte-derived dendritic cells (DCs) and
48 monocyte-derived macrophages, are highly plastic innate immune cells that adopt distinct
49 functional features depending on the extracellular cues they receive. When MCs enter tumors, they
50 respond to signals from the tumor microenvironment (TME) and differentiate into tumor
51 associated macrophages (TAMs), where they promote tumor progression by suppressing anti-
52 tumor T cell and NK cell responses, and by increasing angiogenesis, tumor cell proliferation and
53 metastasis (1-3). In other contexts, such as during acute viral infections, MCs enter inflamed
54 tissues and respond to proinflammatory cytokines such as type I interferons (IFN-I). These
55 inflammatory monocytic lineage cells (infMCs) help mount effective innate and adaptive immune
56 responses through antigen presentation, co-stimulation, and cytokine production (4-9).

57

58 The cyclic GMP-AMP synthase-stimulator of interferon genes (cGAS-STING) pathway elicits an
59 immune response upon the detection of cytosolic DNA.(10-13) Upon binding of double-stranded
60 DNA, cGAS catalyses the formation of 2'3' cyclic GMP-AMP (cGAMP) from cytosolic ATP and
61 GTP molecules (12, 13). cGAMP then binds to the STING adaptor located in the endoplasmic
62 reticulum membrane. This activates NF-κB and IRF3 transcriptional pathways, leading to the
63 production of IFN-Is and other pro-inflammatory cytokines that drive immune responses against
64 viral infection and cancer (10-13).

65

66 Sensing of tumor cell-derived DNA via the cGAS-STING pathway in antigen presenting cells is
67 required for spontaneous priming of anti-tumor $CD8^+$ T cells (14). Moreover, DNA sensing
68 through STING and IFN-I production is required for anti-tumor immune responses induced by

69 radiation therapy and chemotherapy (15). These findings prompted the development of small
70 molecules that could activate the STING-IFN-I pathway for cancer immunotherapy. Activation of
71 STING-IFN-I pathway for cancer immunotherapy has shown promising results in pre-clinical
72 mouse models (16-23). However, to date, clinical trials of STING agonists as monotherapy have
73 shown disappointing results (24), highlighting the need to fully understand the mechanisms of
74 protection in the mouse models to facilitate design of optimized combination therapies. ADU-
75 S100 is a synthetic STING agonist that binds to and activates mouse and human STING and leads
76 to downstream IFN-I production (16, 18). Intra-tumoral administration of ADU-S100 induces
77 tumor regression and systemic protection against tumor re-challenge in mice (16, 18). This effect
78 is mediated through $CD8^+$ T cells and/or NK cells depending on tumor-specific features such as
79 MHC class I expression (16, 21). $BATF3^+$ DCs and IFN-I signaling in cDCs are also required for
80 optimal response to treatment, due to their role in cross-presentation and IL-15 trans-presentation
81 (16, 21). There is a well-established role for IFN-I signaling in the response to STING agonist
82 therapy, as IFNAR1 deficiency or IFN-I neutralization significantly impairs tumor control, $CD8^+$
83 T cell and NK cell responses upon treatment (16, 18, 21).
84
85 Depletion of phagocytic cells using clodronate liposomes can reduce the therapeutic efficacy of
86 STING agonist therapy, suggesting that monocytes and/or macrophages are required for the anti-
87 tumor effects of STING agonists (23, 25, 26). Tumor monocytes accumulating in tumors show
88 transcriptional changes following intra-tumoral STING agonist administration (23, 25, 26).
89 Moreover, monocyte depletion impairs STING-dependent radiation therapy (26). However, to
90 what extent these changes are driven by intrinsic IFN-I signaling and whether IFN-I responses in

91 monocytic lineage cells are required for the therapeutic efficacy of synthetic STING agonists has
92 not been directly tested.
93
94 To address these questions, we investigated the role of intrinsic IFN-I signaling in MCs during
95 intra-tumoral STING agonist therapy of B16F10 tumors using single cell approaches and
96 multiparameter flow cytometry. We report that intra-tumoral injection of ADU-S100 drives the
97 accumulation of $CD26^{lo}CD11b^{+}Ly6C^{hi}CD64^{+}MAR\text{-}1^{+}$ infMCs in the lymph nodes (LNs) and
98 tumors of mice. CITE-sequencing of LN and tumor cells from IFNAR1 mixed bone marrow
99 chimeric mice shows that infMCs that accumulate following STING agonist administration have
100 a transcriptional program almost entirely dependent on intrinsic IFN-I signaling and characterized
101 by high expression of IL-18 and genes involved in MHC I-restricted presentation. *Ccr2*$^{-/-}$ and
102 *Ifnar1*$^{fl/fl}$ *Lyz2-Cre* mice show impaired response to STING agonist therapy compared to littermate
103 controls, suggesting that MC and intrinsic IFN-I responses in these cells are required for optimal
104 response to treatment. Mechanistically, we found that neutralization of IL-18 reduced the
105 therapeutic efficacy of STING agonists in *Ccr2*$^{+/+}$ but not *Ccr2*$^{-/-}$ mice, highlighting the
106 importance of this monocyte-derived pro-inflammatory cytokine during STING agonist therapy of
107 cancer. Taken together, these data suggest that recruitment of MCs and IFN-I-induced IL-18
108 production by infMCs are pivotal for control of melanoma following STING agonist therapy.
109
110
111
112
113

114 **MATERIALS AND METHODS**

115 *Mice.* C57BL/6 and CD45.1 mice were purchased from Charles River Laboratories. *Ifnar1*$^{-/-}$, *Ccr2*$^{-}$
116 $^{/-}$, *Ifnar1*$^{fl/fl}$ and *Lyz2-Cre* mice were purchased from The Jackson Laboratory. *Ccr2*$^{+/-}$ mice were
117 bred to generate *Ccr2*$^{+/+}$ and *Ccr2*$^{-/-}$ littermate controls. *Ifnar1*$^{fl/fl}$ and *Lyz2-Cre* mice were crossed
118 to generate *Ifnar1*$^{fl/fl}$ and *Ifnar1*$^{fl/fl}$ *Lyz2-Cre* littermate controls. Age and sex-matched male and
119 female mice between 6 and 10 weeks of age were enrolled in experiments. Mice were housed
120 under specific pathogen-free conditions. Animal studies were approved by the animal care
121 committee of the University of Toronto in accordance with the Canadian Council on Animal care.
122

123 *Cell culture*. B16F10 cells obtained from the American Type Culture Collection and B16F10.OVA
124 (B16.OVA) was obtained from Dr. Mikael Karlsson, Karolinska Institute. B16.OVA.tomato was
125 generated using the Sleeping Beauty transposon system (Addgene #60513). The MC-38 cell line
126 was obtained from Dr Jean Gariépy at the Sunnybrook Research Institute, Toronto. The cell lines
127 were maintained at 37ºC with 5% CO2 in complete Dulbecco's modified Eagle's medium [10%
128 heat-inactivated fetal bovine serum (FBS), streptomycin (100 mg/ml), and penicillin (100 mg/ml);
129 Gibco].
130

131 *In vivo tumor experiments*. Mice were anesthetized with 2-3% isoflurane and 10^6 B16.OVA, $2x10^6$
132 B16.OVA.tomato or 0.5 x 10^6 MC-38 cells were inoculated intradermally or subcutaneously on
133 the right flank in 50 µl D-PBS. Where relevant, mice were randomized into groups with similar
134 average tumor sizes on the day of treatment. When tumors reached an average volume of 100 mm^3,
135 25 µg of ADU-S100 (MedChemExpress) was administered intratumorally in 50 µl D-PBS. An
136 equal volume of DMSO dissolved in D-PBS was used as vehicle control. Tumor volumes were

137 determined with calipers and the formula (length x width^2) x 0.5. Mice were euthanized when
138 tumors reached >1500 mm^3 or were severely ulcerated. For CCR5 blocking experiments,
139 B16.OVA.tomato tumor-bearing C57BL/6 mice were given 10mg/kg maraviroc or PBS treatment
140 4 hours prior to ADU-S100 or vehicle treatment. LNs were collected for flow cytometry on day 1
141 post-treatment.
142
143 *Tissue processing*. Tumors were resected and cut into small pieces and digested in 1 ml HBSS
144 with 825 U/ml collagenase IV (Invitrogen) and 0.1 mg/ml DNAse I for 30 min at 37°C 250 rpm.
145 Tumor cell suspensions were mashed through a 70 µM strainer, washed once in RPMI 10% FBS
146 and resuspended at 100 mg of tumor/ml in D-PBS. Tumor-draining inguinal LNs on the same side
147 as the tumor were mechanically disrupted through a 70 µM strainer to obtain single-cell
148 suspensions.
149
150 *Flow cytometry*. For flow cytometry, 2 x 10^6 cells from the LN or 25 mg of tumor were used per
151 stain. Cells were stained for 15 minutes in eF506 Viability Dye diluted in D-PBS, washed, and
152 treated with Fc-receptor blocking antibodies anti-CD16/CD32 for 10 minutes (Invitrogen). Cells
153 were then stained with cell surface antibodies for 30 minutes, washed and fixed for 10 minutes in
154 Cytofix buffer (BD) at 4ºC. For tetramer staining, cells were stained for 30 minutes with H-
155 2K^b/SIINFEKL-APC tetramers at room temperature before carrying out cell surface staining as
156 described above. Anti-CD8a clone KT15 was used when staining with tetramers to prevent non-
157 specific binding of H-2K^b tetramers that can occur with clone 53-6.7. For intracellular staining,
158 cells were fixed and permeabilized with Cytofix/Cytoperm buffer (BD) for 20 minutes (for
159 cytokine staining), or the Foxp3 transcription factor staining buffer (Invitrogen) for 40 minutes

160 (for nuclear proteins), prior to intracellular staining for 30 minutes at 4ºC. Data were acquired on
161 a LSR Fortessa X-20 using FACSDiva software (BD Biosciences) and analyzed with FlowJo
162 (TreeStar). Absolute cell numbers in samples were determined using 123count eBeads
163 (Invitrogen).
164
165 *Ifnar1 mixed bone marrow chimeras.* CD45.1/.2 mice were irradiated with two doses of 550 rad
166 with a 4h rest between doses, and the bone marrow was reconstituted by intravenous injection of
167 a 1:1 mixture of *Ifnar1*$^{+/+}$ CD45.1 and *Ifnar1*$^{-/-}$ CD45.2 bone marrow cells for a total of 5x10^{6}
168 cells/mouse. Mice were fed neomycin sulfate water (2 mg/ml) for two weeks following irradiation.
169 Chimerism was assessed in the blood >90 days later, prior to tumor cell inoculation.
170
171 *Sample preparation for CITE-sequencing. Ifnar1* mixed bone marrow chimeras were inoculated
172 with 10^{6} B16.OVA cells intradermally and a single dose of ADU-S100 was administered
173 intratumorally on day 12. LNs and tumors were harvested at day 1 and day 2 post-treatment,
174 respectively. LNs were processed as described above. Tumors were digested in HBSS 875 U/ml
175 collagenase IV for 20 min at 37°C 250 rpm, filtered through 70 µM strainers, centrifugated and
176 resuspended at 120 mg/ml in D-PBS. For both the tumor and LN, equal amounts of cell suspension
177 from 3 vehicle or 3 ADU-S100-treated mice were pooled into one vehicle sample and one ADU-
178 S100 sample. Cells were stained with eF506 fixable viability dye in PBS for 10 min on ice, then
179 washed. Fc Receptors were blocked for 10 min before staining with fluor-conjugated antibodies
180 (for FACS) and TotalSeq-A antibodies (Biolegend) in D-PBS 2% FBS for 25 min on ice. Here,
181 vehicle and ADU-S100 treated samples were labeled with distinct hashtag antibodies, while anti-
182 CD45.1 and anti-CD45 barcoded antibodies were used to label *Ifnar1*$^{+/+}$ and *Ifnar1*$^{-/-}$ cells. Cells

183 were washed three times with D-PBS and sorted on a BD FACS Aria IIu (tumor: live $CD45^+$ cells;
184 LN: live CD3- CD19- $CD11b^+$ and/or $MHCII^+$ cells). Vehicle and ADU-S100-treated samples
185 were pooled together at a 1:1 ratio immediately before partitioning on the 10X chromium
186 controller. The Chromium Single Cell 3' Reagent Kits v3.1 were used according to the
187 manufacturer's user guide in conjunction with CITE-seq & Cell Hashing Protocol from the New
188 York Genome Center Technology Innovation Lab. Of note, anti-CD45 clone I3/2.3, anti-CD45
189 clone 30-F11 (in hashtag antibodies), anti-CD45.1 (clone A20) and anti-CD45.2 (clone 104) did
190 not significantly interfere with each other under our experimental conditions.
191
192 *CITE-sequencing analysis.* Sequencing reads from the mRNA library were processed through the
193 Cell Ranger Single Cell Software Suite (10x Genomics) to obtain gene-cell expression matrices.
194 Antibody-derived tags and hashtags were counted using CITE-seq count v1.4.2 and loaded into
195 the Seurat object. RNA, ADT, and HTO expression matrices were imported into RStudio, and
196 downstream analysis was performed using Seurat v3. Cells that expressed fewer than 500 or more
197 than 7000 genes and had a percentage of mitochondrial genes over 10% were filtered out. RNA
198 counts were log-normalized, while antibody-derived counts were normalized using centered log
199 ratio transformation. The 2000 most variable genes were used for dimensionality reduction using
200 principal component analysis. An elbow plot was used to identify the principal components that
201 contribute to most of the variation. For the LN sample, we used the FindNeighbors function using
202 10 dimensions and ran the FindClusters function with a resolution of 0.5. For the tumor sample,
203 we used the FindNeighbors function using 15 dimensions and ran the FindClusters function with
204 a resolution of 0.5. Contaminating T cell, B cell, pDC, NK cell and neutrophil clusters were
205 excluded from the samples and remaining cells were used for analysis. Differential gene

206 expression analysis was performed in Seurat. Genes were considered significantly differentially
207 expressed when they had a $\log_2$ fold-change of > 0.25 and an adjusted p. value < 0.05. To identify
208 enriched gene sets, genes that were differentially expressed across monocyte/macrophage clusters
209 were used as an input for overrepresentation analysis in g: Profiler using Gene Ontology:
210 Biological processes gene sets. The SCENIC workflow was used to predict gene regulatory
211 networks (27). NicheNet was used to predict receptor ligand interactions between cell types (28).
212
213 *In vivo IL-18 blockade.* Mice were administered 200 µg of anti-IL-18 (clone YIGIF74-IG7,
214 BioXCell) or isotype control (clone 2A3, BioXCell) in 100 µl D-PBS intraperitoneally one day
215 before and one day after STING agonist administration.
216
217 *Statistical analysis.* Data were analyzed in GraphPad Prism software (v9.3.1). Student's t-test or
218 one-way ANOVA were used to determine statistical significance as indicated in figure legends.
219 Tumor growth curves were compared using two-way ANOVA with Sidak's multiple comparisons
220 test; the p-value at the last time point is reported. *P < 0.05, **P < 0.01, ***P < 0.001, and ****P
221 < 0.0001 were applied.
222
223 *Data availability statement.* Sequencing data will be made available on gene expression omnibus
224 (GEO). Other data such as flow cytometry FCS files and tumor growth data are available from the
225 authors upon request.
226
227
228

229 **Results**

230 *STING agonist treatment induces distinct temporal peaks of MC accumulation in tumors and*
231 *lymph nodes, respectively*

232 Changes in myeloid cell populations in the tumors and tumor-draining LNs of mice were analyzed
233 by flow cytometry following intra-tumoral injection of the STING agonist ADU-S100 into pre-
234 established intradermal B16F10.OVA tumors (**Figure 1A**). One day post-treatment, the number
235 and percentage of migratory cDC1 ($CD26^{+}MHCII^{\mathbf{hi}}CD11c^{+}XCR1^{+}$), migratory cDC2
236 ($CD26^{+}MHCII^{\mathbf{hi}}CD11c^{+}CD172^{+}$) and $Ly6C^{hi}$ MCs ($CD26^{-}CD11b^{+}Ly6G^{-}Ly6C^{hi}$) was
237 significantly increased in the LNs but decreased in the tumors (**Figure 1 B-D, F-G**). However, the
238 number of $Ly6C^{hi}$ MCs in the tumors was restored to initial levels by day 2 post-treatment (**Figure**
239 **1F**). $Ly6C^{hi}$ MCs in the LN and tumor were $CD26^{-}CD88^{+}$ whereas cDCs were $CD26^{hi}CD88^{-}$
240 (**Figure S1A, B**), supporting that these are monocytic lineage cells rather than inflammatory cDCs
241 (29).

242

243 CD64 and MAR-1 staining can be used to identify infMCs in mice, as these antibodies label cells
244 that have responded to inflammatory cytokines and PAMPS (29). While CD64 is an Fc receptor
245 upregulated by monocytes in response to IFN-Is and other pro-inflammatory stimuli, MAR-1 is an
246 antibody clone raised against FcεR1 but that was later found to bind to other Fc receptors including
247 CD64 (29, 30). Here, we used these markers to identify cells that had potentially responded to
248 IFN-Is downstream of intra-tumoral STING agonist administration. We also noted that both the
249 cDC and the $Ly6C^{hi}$ MCs had higher levels of MHC I after ADU-S100 compared to vehicle
250 control, consistent with an IFN-I dependent response (**Figure S1C**). The number and percentage
251 of $Ly6C^{hi}$ MCs positive for CD64 and MAR-1 were significantly increased in the LNs and tumors

252 following STING agonist therapy and peaked at 1- and 2-days post-treatment, respectively (**Figure**
253 **1E, H**). Thus, despite an initial decrease in the number of Ly6C^{hi} MCs in the tumor at day 1 post-
254 treatment, the absolute number of infMCs in tumors was increased by day 2 post-treatment
255 compared to baseline. Taken together, these data show that intra-tumoral administration of ADU-
256 S100 drives the accumulation of CD64^{+} MAR-1^{+} infMCs in the LNs and tumors.
257
258 The ability of Ly6C^{hi} MCs to migrate from tissues to the LN and cross-present antigens during
259 viral infection has been questioned (29, 31). To test if the significantly increased number of Ly6C^{hi}
260 MCs in the LN on day 1 following STING agonist therapy was due to migration from the tumors,
261 wild-type mice were inoculated with B16F10.OVA (B16.OVA) cells that express the red
262 fluorescent protein TdTomato (B16.OVA.tomato) and treated with ADU-S100 or vehicle (**Figure**
263 **1I**). In these mice, intra-tumoral STING agonist injection led to a substantial increase in the
264 number and percentage of tomato^{+} CD26^{-}CD11b^{+}Ly6G-Ly6C^{hi} MCs in the LN (**Figure 1J-K**).
265 We also observed a smaller increase in the number and percentage of tomato^{+} cDC2 (**Figure 1J-**
266 **K**).
267
268 Maraviroc is a CCR5 antagonist that has been shown to block CCR5-dependent monocyte
269 trafficking to the LNs (32). Therefore, to determine if CCR5 plays a role in trafficking of the
270 tomato^{+} CD26^{-}CD11b^{+}Ly6G-Ly6C^{hi} MCs from the tumor to the LN, we treated wild-type mice
271 bearing B16.OVA.tomato tumor with maraviroc or vehicle control, then 4 hours later with ADU-
272 S100 or vehicle and monitored tomato^{+} in the tumor dLN at 24 hours (**Figure 1L**). Consistent with
273 a role for CCR5 in migration of monocytes to LNs, maraviroc treatment substantially reduced
274 accumulation of the tumor antigen bearing monocytes to the dLN (**Figure 1M**). We also noted that

275 LN monocytes from STING agonist treated mice express higher CCR5 than cDC1 and cDC2 at 1
276 day after STING agonist treatment (**Figure 1N**). Taken together, these data suggest that STING
277 agonist treatment induced accumulation of monocytic lineage cells in LN and tumor at different
278 time points, and monocytic lineage cells carry tumor protein to the tumor-draining LN in a CCR5-
279 dependent manner.
280
281 *infMCs are required for optimal tumor control following intra-tumoral STING agonist injection*
282 CCR2 signaling is required for exit of monocytes from the bone marrow (33, 34). To test if CCR2-
283 dependent infMCs play a role in the tumor control induced by STING agonists, we tracked the
284 growth of B16.OVA and MC-38 tumors in *Ccr2*$^{+/+}$ and *Ccr2*$^{-/-}$ littermate mice treated with ADU-
285 S100 or vehicle control. In contrast to *Ccr2*$^{+/+}$ mice, infMCs do not accumulate in the tumors of
286 *Ccr2*$^{-/-}$ mice after STING agonist therapy (**Figure 2A**), whereas tumor accumulation of other
287 immune cell types was unaffected (**Figure S2A, B**). While *Ccr2*$^{+/+}$ and *Ccr2*$^{-/-}$ mice treated with
288 the vehicle control showed no differences in tumor growth, *Ccr2*$^{-/-}$ mice showed impaired tumor
289 control compared to *Ccr2*$^{+/+}$ mice following STING agonist therapy (**Figure 2B, C**).
290
291 STING agonist therapy induces the expansion of tumor specific CD8^{+} T cell and NK cell
292 populations which are measurable as early as 3 days post-treatment (18, 21). To test if monocytes
293 contribute to the proliferation of tumor-specific T cells and NK cells, *Ccr2*$^{+/+}$ and *Ccr2*$^{-/-}$ mice with
294 B16.OVA tumors were sacrificed 3 days post-treatment with STING agonists or vehicle control
295 for flow cytometry analysis. STING agonists significantly increased the proportion of H-2K^{b}
296 SIINFEKL^{+} CD8^{+} T cells and NK cells proliferating in the LN based on Ki-67 staining (**Figure**
297 **2D, E and Figure S2C**). *Ccr2*$^{-/-}$ mice showed reduced Ki67^{+} NK cells (% and mean fluorescence

298 intensity, MFI), but there was no impact on the absolute number of Ki67^{+} NK cells in LN and
299 tumor (**Figure 2E and S2C**). For T cells, although the MFI for Ki67 was decreased in CCR2$^{-/-}$
300 mice, neither the frequency or absolute number of Ki67^{+} cells was significantly impacted by CCR2
301 (**Figure 2D and S2C**). These results may be confounded by the significant apoptosis of
302 lymphocytes in tumors early after ADU-S100 treatment (35). At later time points rapid tumor
303 shrinkage in the *Ccr2*$^{+/+}$ mice precluded accurate T cell measurements. Therefore, to further
304 investigate whether *Ccr2*-deficiency affects early T cell proliferation, we adoptively transferred
305 OT-I T cells into *Ccr2*$^{+/+}$ or *Ccr2*$^{-/-}$ B16.OVA tumor bearing mice 1 day prior to ADU-S100
306 treatment. However, there was no significant impact of *Ccr2* on LN OT-I T cell proliferation
307 (**Figure S2D**). These data suggest that CCR2-dependent MCs contribute to tumor control but have
308 little or no impact on the priming or initial proliferation of the tumor-specific T cells.
309
310 *InfMCs are driven by intrinsic IFN-I signalling during STING agonist therapy*
311 Mice deficient for the interferon alpha/beta receptor 1 (IFNAR1) have sub-optimal responses to
312 STING agonists,(16, 18) but whether IFNAR1 signaling within the monocytes promotes anti-
313 tumor immunity in this context is unknown. To address this question, we tracked the growth of
314 B16.OVA tumors in *Ifnar1*$^{fl/fl}$ *Lyz2-Cre* mice, which have lower expression of IFNAR1 on myeloid
315 cells, including monocytes (**Figure 3A, B**). *Ifnar1*$^{fl/fl}$ *Lyz2-Cre* mice showed increased tumor
316 growth following STING agonist treatment compared to ADU-S100 *Ifnar1*$^{fl/fl}$ littermate controls
317 (**Figure 3C**). These data suggest that IFN-I responses in infMCs are required for optimal tumor
318 control in the presence of STING agonists.
319

320 To more directly test if infMCs were driven by IFN-I, we analysed responses to STING agonist
321 therapy in mixed bone marrow chimeras in which the hematopoietic cells were derived from a 1:1
322 mix of *Ifnar1*$^{+/+}$ or *Ifnar1*$^{-/-}$ bone marrow cells (**Figure 3D**). The increase in numbers of cDC1,
323 cDC2 and Ly6C^{hi} MCs in the LN at day 1 following STING agonist therapy was largely
324 independent of intrinsic IFN-I signaling (**Figure 3E**). However, upregulation of inflammatory
325 markers CD64 and MAR-1 by Ly6C^{hi} MCs in the LN and tumor was mainly restricted to the wild-
326 type compartment of the chimeric mice (**Figure 3F-H**). These data indicate that intrinsic IFN-I
327 signaling drives an inflammatory phenotype in Ly6C^{hi} MCs but is not required for MC migration
328 to the LN during STING agonist therapy.
329
330 To define how intrinsic IFN-I signalling downstream of intratumoral STING agonist treatment
331 alters the transcriptional state of myeloid cells, CITE-sequencing was performed on immune cells
332 derived from the LNs and tumors of *Ifnar1* mixed bone marrow chimeric mice treated with ADU-
333 S100 or vehicle control (**Figure 4A**). Mice were reconstituted with a 1:1 mix of *Ifnar1*$^{+/+}$ and
334 *Ifnar1*$^{-/-}$ bone marrow cells, and chimerism in the blood was confirmed after 90 days later (**Figure**
335 **S3A, B**). At 12 days following tumor inoculation, mice were treated with ADU-S100 or vehicle
336 and LNs and tumors were harvested 1 day and 2 days post-treatment, respectively. To enrich for
337 myeloid cells, CD3-CD19-CD11b^{+} and/or MHCII^{+} cells were sorted from the LN. Because the
338 tumors are already enriched for myeloid cells, total CD45^{+} cells were sorted from tumors (**Figure**
339 **S3C).** Here, DNA-barcoded antibodies were used to trace the treatment group (vehicle or ADU-
340 S100) and the genotype (*Ifnar1*$^{+/+}$ or *Ifnar1*$^{-/-}$) of each single cell based on the sequencing data
341 (**Figure S3D, E**). After quality filtering, 12, 078 and 3001 cells from the LN and tumor,
342 respectively, remained for downstream analysis (**Figure S3F**). As expected, cells assigned as

343 *Ifnar1*$^{-/-}$ cells expressed very low levels of ISGs compared to *Ifnar1*$^{+/+}$, and ISG expression levels
344 were higher in cells derived from the ADU-S100-treated group compared to vehicle, validating
345 the demultiplexing strategy (**Figure S3G**).
346
347 Clusters of monocytes/macrophages (MC/MP) (CD88/*C5ar1*, CD11b/*Itgam*), cDC1 (XCR1/*Xcr1*,
348 CD26/*Dpp4*) and cDC2 (CD172/*Sirpa*, CD26/*Dpp4*) were identified in the LN and tumor (Figure
349 4B-C). LN cDCs also expressed high levels of *Ccr7*, as opposed to monocytes, which expressed
350 *Ccr2* and *Ccr5* (**Figure 4B-C**). Each cell type could be further subdivided into subclusters that
351 represent different transcriptional states. Clusters MC_1, cDC1_1 and cDC2_1 in the LN and
352 cluster MC/MF_1 in the tumor were almost exclusively derived from the *Ifnar1*$^{+/+}$ compartment
353 of the STING agonist treated chimeric mice (**Figure 4D**). These clusters shared a common IFN-I
354 gene signature with high expression of interferon signaling genes (ISGs) including *Isg15*, *Isg20*,
355 *Irf7*, *Ifit1*, *Ifi35* and *Bst2* (**Figure 4E-F**). The proportion of MC/MPs with this inflammatory
356 signature was substantially higher in the STING agonist-treated mice compared to controls
357 (**Figure 4G**). Moreover, this state was entirely dependent on intrinsic IFN-I signalling as no *Ifnar1*$^{-}$
358 $^{/-}$ cells were found in these clusters (**Figure 4G**). Because clusters MC_1, cDC1_1 and cDC2_1 in
359 the LN and MC/MP_1 in the tumor are driven by IFN-Is, we will refer to them as infMCs, infDC1
360 and infDC2.
361
362 In the LN and tumor, cells in cluster MC_2 were almost uniquely derived from the *Ifnar1*$^{-/-}$
363 compartment of STING agonist-treated mice, suggesting this state is induced by STING agonist
364 therapy in the absence of intrinsic IFN-I signalling (**Figure 4D**). Cells from clusters MC/MP_3
365 and MC/MP_4 in the tumor were derived from both treatment groups and genotypes, indicating

366 these states are not driven by STING agonist therapy or IFN-I signaling (**Figure 4D**). Cluster
367 MC/MP_4 expressed genes associated with pro-tumorigenic TAMs such as *Vegfa*, *Arg1* and
368 *Cd274* (**Figure 4H**). Pathways associated with cells in tumor cluster MC/MP_4 include
369 "Angiogenesis" and "TGF-β production", suggesting they play a pro-tumorigenic role (**Figure 4I**).
370 The proportion of MC/MP4s was reduced upon STING agonist therapy in a IFN-I-dependent
371 manner (**Figure 4G**). LN and tumor monocyte derived cells also showed IFNAR-1 dependent
372 increases in MHC I genes, along with TAP and proteasome genes (**Figure 4J**). Taken together,
373 these data show that intrinsic IFN-I signaling reduces pro-tumorigenic gene signatures while
374 enhancing genes associated with antigen presentation and inflammatory cytokine production in
375 monocyte-derived cells.
376
377 *InfMCs have a unique inflammatory gene signature compared to infDCs*
378 Inflammatory gene signatures of infMCs, infDC1 and infDC2 were determined by differential
379 gene expression analysis between inflammatory and non-inflammatory subclusters. A core set of
380 214 inflammatory genes were shared between infMCs, infDC1 and infDC2 (**Figure 5A**). These
381 included common ISGs such as *Isg15*, *Isg20* and *Ifit1*. Inflammatory genes that were more highly
382 expressed by infMCs included the cytokine *Il18*, the chemokines *Ccl2*, *Cxcl9* and *Cxcl10*, cell
383 surface molecules *Fcgr1* and *Ly6c2*. In contrast, infDCs expressed higher levels of *Il15*, *Cd70*,
384 *CD86* and *Cd274* (**Figure 5B**). Regulatory network inference predicted that the inflammatory
385 programs in infMCs, infDC1 and infDC2 are driven by different transcriptional regulators
386 downstream of IFN-I signaling. While infMCs were driven by ISGF3 (*Stat1*, *Stat2* and *Irf9*), *Irf5*
387 and *Irf7*, infDCs were predominantly driven by NF-κB family members (*Nfkb2*, *Rel*, *Relb*), *Stat3*,
388 *Stat4* and *Klf6* (**Figure 5C**).

389

390 By comparing the changes in gene expression between monocytes and macrophages from vehicle
391 and STING-agonist treated mice within the *Ifnar1*$^{+/+}$ and *Ifnar1*$^{-/-}$ compartments, we identified a
392 set of genes that were upregulated upon STING agonist therapy in both the *Ifnar1*$^{+/+}$ and *Ifnar1*$^{-/-}$
393 compartments (**Figure S4**). These included genes involved in the complement system (*C1qa,*
394 *C1qb, C1qc*, *C3ar1*), genes associated with lysosomes including cathepsins (*Ctsb, Ctsc, Ctsd, Ctsl*)
395 and *Lamp1*, as well as genes encoding for the transcription factors *Fosb* and *Maf* (**Figure S4**).

396

397 *Il18 is induced by IFN-I signalling in monocytic lineage cells and is important for the anti-tumor*
398 *response to STING agonists*

399 Receptor-ligand interactions between infMCs and CD8^{+} T cells or NK cells were predicted using
400 NicheNet. (28) IL-18 – IL-18R1 interaction was the top predicted interaction between infMCs and
401 CD8^{+} T cells or NK cells (**Figure 6A**). *Il18* expression was specifically upregulated by infMCs
402 and not by infDC1 or infDC2 (**Figure 6A**). IL-18R1 was highly expressed on both tumor-specific
403 CD8^{+} T cells and NK cells in the lymph node and tumor and was upregulated on tumor-specific
404 CD8^{+} T cells upon STING agonist therapy (**Figure 6B-C).** Accordingly, blockade of IL-18 using
405 a neutralizing antibody led to impaired tumor control in mice treated with ADU-S100 (**Figure**
406 **6D**), in line with previous studies that show that activation of the IL-18-IL-18R pathway promotes
407 CD8^{+} T cell and NK cell responses against tumors (36, 37). To determine the contribution of
408 monocyte derived IL-18 to tumor control, we compared the effect of blocking IL-18 with anti-IL-
409 18 antibody in *Ccr2*$^{+/+}$ or *Ccr2*$^{-/-}$ mice (**Figure 6E**). Whereas anti-IL-18 increased tumor growth
410 in WT mice, tumor growth was not impacted by anti-IL-18 in CCR2$^{-/-}$ mice consistent with a role

411 for infMC in provision of IL-18. Taken together these data support an anti-tumor role for
412 monocyte-derived IL-18 in STING agonist therapy.
413
414

415 **DISCUSSION**

416 MCs often acquire pro-tumorigenic features in the TME in response to factors such as hypoxia and
417 fibrosis. Therefore, therapeutic strategies have aimed to either deplete these populations or
418 reprogram them towards more pro-immunogenic states (38). The latter approach may be
419 preferable, as it takes advantage of the anti-tumorigenic features of MCs that are non-redundant
420 with that of other immune cells. STING agonist treatment promotes recruitment of MCs, and the
421 IFN-I production induced by STING agonists drives intrinsic phenotypical, transcriptional, and
422 functional changes in the MC, associated with tumor control.

423

424 We show here that *Ccr2*$^{-/-}$ mice have impaired responses to STING agonist therapy compared to
425 *Ccr2*$^{+/+}$ littermates. CCR2 is required for monocyte egress from the bone marrow, and *Ccr2*$^{-/-}$ mice
426 lack circulating monocytes (33, 34). Although we cannot exclude that *Ccr2*$^{-/-}$ mice might also have
427 defects in the CCR2-dependent migration of other cell populations, the finding that CCR2-
428 deficiency did not impact overall numbers of cDC1 or cDC2, is consistent with monocytes playing
429 a role in STING agonist therapy. Previous studies have reported reduced response to STING
430 agonists in cancer models when mice are treated with chlodronate liposomes (23, 25), which
431 deplete phagocytic cells including macrophages and MCs. Our results complement these studies
432 by suggesting a more specific role of CCR2-dependent MCs, as opposed to tissue macrophages,
433 during STING agonist therapy of cancer and by investigating the intrinsic role of IFN-I signaling
434 in these cells.

435

436 Our experiments using *Ifnar1*$^{fl/fl}$ *Lyz2-Cre* mice indicate that intrinsic IFN-I signaling in *Lyz2*$^{+}$ cells
437 contribute to tumor control in the presence of STING agonists. *Lyz2*-cre is expected to delete

438 floxed genes in approximately 40-50% of blood monocytes with less than 10% deletion in cDCs
439 (39). Accordingly, we observed a significant loss of cell surface IFNAR1 expression on tumor-
440 infiltrating Ly6C^{hi} MCs in *Ifnar1*$^{fl/fl}$ *Lyz2-Cre* compared to *Ifnar1*$^{fl/fl}$ controls. This loss of IFNAR
441 expression was sufficient to significantly reduce cell surface expression of the IFN-I regulated
442 protein CD64 on these cells, validating that this mouse model is relevant to study the role of IFN-
443 I responses in Ly6C^{hi} MCs. While we cannot exclude that IFN-Is in other *Lyz2*$^{+}$ cells such as
444 neutrophils might also contribute to the response to STING agonist therapy, these data combined
445 with the experiments using *Ccr2*$^{-/-}$ mice are compatible with a role for IFN-I signaling in
446 monocytes during STING agonist therapy of cancer.
447
448 Some studies have shown a role for monocytes as a source of STING induced IFN-I. For
449 example, Lam et al showed that microbiota-derived STING agonists induced by a high fat diet
450 induced IFN-I production by tumor monocytes to promote DC-NK cell crosstalk (40). Monocytes
451 were also recently found to be the main source of IFN-I after radiation therapy of mice (26),
452 whereas another recent study showed that tumors are the major source of STING-dependent IFN-
453 I in mouse and human cancers (26, 41). We did not observe *Ifn* production by monocytes in our
454 RNA-sequencing data at day 2 post-treatment, albeit we did not further pursue the source of IFN-
455 I in our model.
456
457 A recent study by Tadepalli et al. used depletion of CCR2 positive cells during radiation therapy
458 of mouse tumors to implicate monocytes in CD8 T cell responses and tumor control in a model in
459 which STING is important for the effects of radiation induced tumor control (26). Conversely,
460 Nicolai et al. used IFNAR1 CD11c-cre mice to show that IFN-I responses in cDCs are required

461 for NK-cell mediated tumor control during STING agonist therapy (21). Our findings are
462 complementary to these previous studies on the role of STING during tumor therapy because
463 they highlight the role of CCR2-dependent cells and intrinsic IFN-I signaling in MCs following
464 intratumoral delivery of STING agonists (18, 21, 26, 40, 41).
465
466 Using IFNAR1 mixed bone marrow chimeric mice, flow cytometry and CITE-sequencing, we
467 showed that intrinsic IFN-I signaling in monocytic lineage cells drives an inflammatory phenotype
468 characterized by positive staining for CD64 and FcεR1 (MAR-1), akin to infMCs observed in
469 models of acute viral infection (4, 5). Transcriptionally, infMCs express high levels of common
470 ISGs, as well as inflammatory cytokines (*Il15*, *Il18*) and chemokines (*Ccl2, Cxcl9, Cxcl10*). This
471 state is also entirely dependent on intrinsic IFN-I signaling, as *Ifnar1*$^{-/-}$ cells within the same mice
472 do not adopt this transcriptional state, despite exposure to the same environmental cues. Skewing
473 of monocyte and macrophage populations towards a more pro-inflammatory phenotype during
474 STING agonist therapy was previously reported (23,25), but whether this was driven by intrinsic
475 IFN-I responses had not been tested. In line with the study by Xu et al. (23) , we also find a loss
476 of TAMs with a pro-tumorigenic transcriptional profile upon STING agonist treatment.
477 Interestingly, we report that the lack of this population in STING agonist treated tumors is
478 dependent on intrinsic IFN-I signaling in monocytes, which to our knowledge had not been shown
479 previously. Although we did not formally confirm the loss of TAM markers at the protein level,
480 our findings are consistent with a recent study showing that intrinsic IFNAR1 signaling prevents
481 the acquisition of immune suppressive features by myeloid-derived suppressor cells (42).
482

483 Based on CD64 and FcεR1 (MAR-1) staining, the inflammatory state of monocytic lineage cells
484 in the LN and tumors was transient, peaking at day 1-2 and returning to baseline by day 5 post-
485 ADU-S100 treatment. Monocytic lineage cells might re-acquire a pro-tumorigenic profile in
486 absence of sustained IFN-I signaling. In a breast cancer model, depletion of TAMs with liposome
487 clodronate during the first week of treatment with CAR-T cells and the STING agonist DMXAA
488 reduced tumor control (23). However, depleting TAMs at later time points helped sustain tumor
489 regression, indicating that TAMs reacquired a suppressive profile over time (23). In this case, an
490 alternative approach to cell depletion could be the use of fractionated treatment regimens where
491 STING agonists are given every 2-3 days, as this might sustain inflammatory states and prevent
492 the resurgence of pro-tumorigenic TAMs.
493
494 Although cDC1 are specialized in the presentation of exogenous antigens, other APC populations
495 including monocytes, have been reported to acquire the ability to cross-prime $CD8^+$ T cells if
496 appropriately stimulated (8, 43-46). However, the idea that infMCs can migrate to the LN and
497 effectively cross-prime $CD8^+$ T cells has recently been challenged (29, 31). The characterization
498 of a population of bona-fide cDC2s that express CD64 and stain positive for MAR-1 (infDC2s)
499 suggested that the observed migration and priming ability of infMCs might have been attributable
500 to contaminating cDCs. To accurately delineate infMCs from infDC2s in mice, it is now
501 recommended to use CD26 and CD88 (29). Here, we report that $CD26^-CD88^+$ $Ly6C^{hi}$ MCs
502 effectively take up tumor proteins and carry them to the LNs in response to intra-tumoral STING
503 agonist administration. These cells were phenotypically and transcriptionally distinct from
504 $CD26^+CD88^-$ infDCs, and expressed conventional monocyte genes such as *Csf1r*, *Ccr2*, *Itgam* and
505 *Plac8*. A possible explanation for these conflicting findings is that we did not pre-gate on $MHCII^{hi}$

506 cells in our analyses of infMCs. As infMCs in the LN express significantly lower levels of MHCII
507 than cDCs, pre-gating on MHCII^{hi} cells might exclude them from the analysis.
508
509 Recently, CCR5 has been implicated in trafficking of monocytes to LNs (32). Consistently, we
510 observed CCR5 protein expression on the monocytes. Moreover, *Ccr5* was identified as a
511 monocyte but not DC expressed gene in the CITE-seq data, and the CCR5 antagonist maraviroc
512 substantially reduced the trafficking of monocytes from the tumor to the dLN. The relevance of
513 trafficking of the infMC to the LN was not further investigated here, however, recent data suggest
514 a role for LN monocytes in interactions with DCs (47).
515
516 We observed strong IFNAR1-dependent increases in MHC I and genes associated with Ag
517 presentation in the CITE-seq data and we observed increased MHC I protein expression on the
518 infMC in response to STING agonist therapy, consistent with increased peptide loading. However,
519 *Ccr2*$^{-/-}$ mice which lack infMC, did not show impairment in proliferation of adoptively transferred
520 OT-I T cells compared to WT mice, arguing that infMCs are not required for T cell priming or
521 early T cell proliferation in this model. These findings are consistent with the observation Batf3^{+}
522 DCs are important for T cell priming during STING agonist therapy of cancer (48). In viral
523 infection models, monocytes have been shown to provide post-priming signals to T cells (4).
524
525 Our data showed that STING agonists induce immunological control of tumors at least in part
526 through increased IL-18 production by monocytes. We confirm the biological relevance of this
527 finding, by showing that in vivo neutralization of IL-18 reduced the efficacy of STING agonists
528 in driving tumor control in *Ccr2*$^{+/+}$ but not *Ccr2*$^{-/-}$ mice. *Il18* was expressed by infMCs which

529 have responded to IFN-I in the tumor and LN after STING agonist therapy. This is in line with
530 previous studies demonstrating that IL-18 is transcriptionally regulated by STING and/or IFN-I
531 signaling (49, 50). IFN-I dependent production of IL-18 by infMCs is also important for immune
532 responses to viral, parasitic, or bacterial infections (6, 7). While *Il18* and intracellular IL-18 levels
533 are upregulated in MCs upon exposure to IFN-Is, IL-18 requires proteolytic cleavage downstream
534 of inflammasome activation to be secreted. There is evidence that the cGAS-STING-IFN-I axis
535 activates the inflammasome in human and mouse MCs (51-53) .
536
537 In conclusion, we have shown that intra-tumoral STING agonist therapy mediates at least part of
538 its effects through infMCs. Mechanistically, STING agonists increased IFN-I signaling in
539 monocytes, driving a unique inflammatory state that includes production of IL-18, which was
540 important for tumor control. Taken together, these findings highlight the importance of infMCs in
541 STING agonist therapy of cancer. Monitoring STING agonist therapy in humans for induction of
542 infMCs and IL-18 could help optimize such therapies.
543
544 **Acknowledgements:** The authors thank Birinder Ghumman for technical assistance; Nathalie
545 Simard and Janine Charron for assistance with fluorescence-activated cell sorting; Dr Slava
546 Epelman and Rysa Zaman for breeding *Ifnar1*$^{fl/fl}$ *Lyz2-Cre* mice; Dr Jean Gariépy for sharing the
547 MC-38 cell line, and Drs. Sonya MacParland and Arthur Mortha for critical reading of the
548 manuscript.
549
550
551

552 **References:**

553 1. DeNardo, D. G., and B. Ruffell. 2019. Macrophages as regulators of tumour immunity
554 and immunotherapy. *Nature Reviews Immunology* 19: 369-382.
555 2. Ugel, S., S. Cane, F. De Sanctis, and V. Bronte. 2021. Monocytes in the Tumor
556 Microenvironment. *Annu Rev Pathol* 16: 93-122.
557 3. Olingy, C. E., H. Q. Dinh, and C. C. Hedrick. 2019. Monocyte heterogeneity and
558 functions in cancer. *J Leukoc Biol* 106: 309-322.
559 4. Chang, Y. H., K. C. Wang, K. L. Chu, D. L. Clouthier, A. T. Tran, M. S. Torres Perez, A.
560 C. Zhou, A. A. Abdul-Sater, and T. H. Watts. 2017. Dichotomous Expression of TNF
561 Superfamily Ligands on Antigen-Presenting Cells Controls Post-priming Anti-viral
562 CD4(+) T Cell Immunity. *Immunity* 47: 943-958 e949.
563 5. Chu, K. L., N. V. Batista, K. C. Wang, A. C. Zhou, and T. H. Watts. 2019. GITRL on
564 inflammatory antigen presenting cells in the lung parenchyma provides signal 4 for T-cell
565 accumulation and tissue-resident memory T-cell formation. *Mucosal Immunol* 12: 363-
566 377.
567 6. Lee, A. J., B. Chen, M. V. Chew, N. G. Barra, M. M. Shenouda, T. Nham, N. van
568 Rooijen, M. Jordana, K. L. Mossman, R. D. Schreiber, M. Mack, and A. A. Ashkar.
569 2017. Inflammatory monocytes require type I interferon receptor signaling to activate NK
570 cells via IL-18 during a mucosal viral infection. *J Exp Med* 214: 1153-1167.
571 7. Soudja, S. M., A. L. Ruiz, J. C. Marie, and G. Lauvau. 2012. Inflammatory monocytes
572 activate memory CD8(+) T and innate NK lymphocytes independent of cognate antigen
573 during microbial pathogen invasion. *Immunity* 37: 549-562.

574 8. Bedford, J. G., M. Heinlein, A. L. Garnham, T. H. O. Nguyen, T. Loudovaris, C. Ge, S. I.
575 Mannering, M. Elliott, S. G. Tangye, K. Kedzierska, D. H. D. Gray, W. R. Heath, and L.
576 M. Wakim. 2020. Unresponsiveness to inhaled antigen is governed by conventional
577 dendritic cells and overridden during infection by monocytes. *Sci Immunol* 5.
578 9. Chu, K. L., N. V. Batista, M. Girard, and T. H. Watts. 2020. Monocyte-Derived Cells in
579 Tissue-Resident Memory T Cell Formation. *J Immunol* 204: 477-485.
580 10. Ishikawa, H., and G. N. Barber. 2008. STING is an endoplasmic reticulum adaptor that
581 facilitates innate immune signalling. *Nature* 455: 674-678.
582 11. Ishikawa, H., Z. Ma, and G. N. Barber. 2009. STING regulates intracellular DNA-
583 mediated, type I interferon-dependent innate immunity. *Nature* 461: 788-792.
584 12. Sun, L., J. Wu, F. Du, X. Chen, and Z. J. Chen. 2013. Cyclic GMP-AMP synthase is a
585 cytosolic DNA sensor that activates the type I interferon pathway. *Science* 339: 786-791.
586 13. Wu, J., L. Sun, X. Chen, F. Du, H. Shi, C. Chen, and Z. J. Chen. 2013. Cyclic GMP-
587 AMP is an endogenous second messenger in innate immune signaling by cytosolic DNA.
588 *Science* 339: 826-830.
589 14. Woo, S. R., M. B. Fuertes, L. Corrales, S. Spranger, M. J. Furdyna, M. Y. Leung, R.
590 Duggan, Y. Wang, G. N. Barber, K. A. Fitzgerald, M. L. Alegre, and T. F. Gajewski.
591 2014. STING-dependent cytosolic DNA sensing mediates innate immune recognition of
592 immunogenic tumors. *Immunity* 41: 830-842.
593 15. Deng, L., H. Liang, M. Xu, X. Yang, B. Burnette, A. Arina, X. D. Li, H. Mauceri, M.
594 Beckett, T. Darga, X. Huang, T. F. Gajewski, Z. J. Chen, Y. X. Fu, and R. R.
595 Weichselbaum. 2014. STING-Dependent Cytosolic DNA Sensing Promotes Radiation-

596 Induced Type I Interferon-Dependent Antitumor Immunity in Immunogenic Tumors.
597 *Immunity* 41: 843-852.
598 16. Corrales, L., L. H. Glickman, S. M. McWhirter, D. B. Kanne, K. E. Sivick, G. E.
599 Katibah, S. R. Woo, E. Lemmens, T. Banda, J. J. Leong, K. Metchette, T. W. Dubensky,
600 Jr., and T. F. Gajewski. 2015. Direct Activation of STING in the Tumor
601 Microenvironment Leads to Potent and Systemic Tumor Regression and Immunity. *Cell*
602 *Rep* 11: 1018-1030.
603 17. Fu, J., D. B. Kanne, M. Leong, L. H. Glickman, S. M. McWhirter, E. Lemmens, K.
604 Mechette, J. J. Leong, P. Lauer, W. Liu, K. E. Sivick, Q. Zeng, K. C. Soares, L. Zheng,
605 D. A. Portnoy, J. J. Woodward, D. M. Pardoll, T. W. Dubensky, Jr., and Y. Kim. 2015.
606 STING agonist formulated cancer vaccines can cure established tumors resistant to PD-1
607 blockade. *Sci Transl Med* 7: 283ra252.
608 18. Sivick, K. E., A. L. Desbien, L. H. Glickman, G. L. Reiner, L. Corrales, N. H. Surh, T. E.
609 Hudson, U. T. Vu, B. J. Francica, T. Banda, G. E. Katibah, D. B. Kanne, J. J. Leong, K.
610 Metchette, J. R. Bruml, C. O. Ndubaku, J. M. McKenna, Y. Feng, L. Zheng, S. L.
611 Bender, C. Y. Cho, M. L. Leong, A. van Elsas, T. W. Dubensky, Jr., and S. M.
612 McWhirter. 2018. Magnitude of Therapeutic STING Activation Determines CD8(+) T
613 Cell-Mediated Anti-tumor Immunity. *Cell Rep* 25: 3074-3085 e3075.
614 19. Chin, E. N., C. Yu, V. F. Vartabedian, Y. Jia, M. Kumar, A. M. Gamo, W. Vernier, S. H.
615 Ali, M. Kissai, D. C. Lazar, N. Nguyen, L. E. Pereira, B. Benish, A. K. Woods, S. B.
616 Joseph, A. Chu, K. A. Johnson, P. N. Sander, F. Martinez-Pena, E. N. Hampton, T. S.
617 Young, D. W. Wolan, A. K. Chatterjee, P. G. Schultz, H. M. Petrassi, J. R. Teijaro, and

618 L. L. Lairson. 2020. Antitumor activity of a systemic STING-activating non-nucleotide
619 cGAMP mimetic. *Science* 369: 993-999.
620 20. Pan, B. S., S. A. Perera, J. A. Piesvaux, J. P. Presland, G. K. Schroeder, J. N. Cumming,
621 B. W. Trotter, M. D. Altman, A. V. Buevich, B. Cash, S. Cemerski, W. Chang, Y. Chen,
622 P. J. Dandliker, G. Feng, A. Haidle, T. Henderson, J. Jewell, I. Kariv, I. Knemeyer, J.
623 Kopinja, B. M. Lacey, J. Laskey, C. A. Lesburg, R. Liang, B. J. Long, M. Lu, Y. Ma, E.
624 C. Minnihan, G. O'Donnell, R. Otte, L. Price, L. Rakhilina, B. Sauvagnat, S. Sharma, S.
625 Tyagarajan, H. Woo, D. F. Wyss, S. Xu, D. J. Bennett, and G. H. Addona. 2020. An
626 orally available non-nucleotide STING agonist with antitumor activity. *Science* 369.
627 21. Nicolai, C. J., N. Wolf, I. C. Chang, G. Kirn, A. Marcus, C. O. Ndubaku, S. M.
628 McWhirter, and D. H. Raulet. 2020. NK cells mediate clearance of CD8(+) T cell-
629 resistant tumors in response to STING agonists. *Sci Immunol* 5.
630 22. McAndrews, K. M., S. P. Y. Che, V. S. LeBleu, and R. Kalluri. 2021. Effective delivery
631 of STING agonist using exosomes suppresses tumor growth and enhances anti-tumor
632 immunity. *J Biol Chem*: 100523.
633 23. Xu, N., D. C. Palmer, A. C. Robeson, P. Shou, H. Bommiasamy, S. J. Laurie, C. Willis,
634 G. Dotti, B. G. Vincent, N. P. Restifo, and J. S. Serody. 2021. STING agonist promotes
635 CAR T cell trafficking and persistence in breast cancer. *J Exp Med* 218.
636 24. Gogoi, H., S. Mansouri, and L. Jin. 2020. The Age of Cyclic Dinucleotide Vaccine
637 Adjuvants. *Vaccines (Basel)* 8.
638 25. Ohkuri, T., A. Kosaka, K. Ishibashi, T. Kumai, Y. Hirata, K. Ohara, T. Nagato, K.
639 Oikawa, N. Aoki, Y. Harabuchi, E. Celis, and H. Kobayashi. 2017. Intratumoral

640 administration of cGAMP transiently accumulates potent macrophages for anti-tumor
641 immunity at a mouse tumor site. *Cancer Immunol Immunother* 66: 705-716.
642 26. Tadepalli, S., D. R. Clements, S. Saravanan, R. Arroyo Hornero, A. Lüdtke, B.
643 Blackmore, J. A. Paulo, A. Gottfried-Blackmore, D. Seong, S. Park, L. Chan, B. J.
644 Kopecky, Z. Liu, F. Ginhoux, K. J. Lavine, J. P. Murphy, M. Mack, E. E. Graves, and J.
645 Idoyaga. 2023. Rapid recruitment and IFN-I–mediated activation of monocytes dictate
646 focal radiotherapy efficacy. *Science Immunology* 8: eadd7446.
647 27. Aibar, S., C. B. Gonzalez-Blas, T. Moerman, V. A. Huynh-Thu, H. Imrichova, G.
648 Hulselmans, F. Rambow, J. C. Marine, P. Geurts, J. Aerts, J. van den Oord, Z. K. Atak, J.
649 Wouters, and S. Aerts. 2017. SCENIC: single-cell regulatory network inference and
650 clustering. *Nat Methods* 14: 1083-1086.
651 28. Browaeys, R., W. Saelens, and Y. Saeys. 2020. NicheNet: modeling intercellular
652 communication by linking ligands to target genes. *Nat Methods* 17: 159-162.
653 29. Bosteels, C., K. Neyt, M. Vanheerswynghels, M. J. van Helden, D. Sichien, N. Debeuf,
654 S. De Prijck, V. Bosteels, N. Vandamme, L. Martens, Y. Saeys, E. Louagie, M. Lesage,
655 D. L. Williams, S. C. Tang, J. U. Mayer, F. Ronchese, C. L. Scott, H. Hammad, M.
656 Guilliams, and B. N. Lambrecht. 2020. Inflammatory Type 2 cDCs Acquire Features of
657 cDC1s and Macrophages to Orchestrate Immunity to Respiratory Virus Infection.
658 *Immunity* 52: 1039-1056 e1039.
659 30. Tang, X. Z., J. B. Jung, and C. D. C. Allen. 2019. A case of mistaken identity: The MAR-
660 1 antibody to mouse FcepsilonRIalpha cross-reacts with FcgammaRI and FcgammaRIV.
661 *J Allergy Clin Immunol* 143: 1643-1646 e1646.

662 31. Coillard, A., and E. Segura. 2021. Antigen presentation by mouse monocyte-derived
663 cells: Re-evaluating the concept of monocyte-derived dendritic cells. *Mol Immunol* 135:
664 165-169.
665 32. Rawat, K., A. Tewari, X. Li, A. B. Mara, W. T. King, S. L. Gibbings, C. F. Nnam, F. W.
666 Kolling, B. N. Lambrecht, and C. V. Jakubzick. 2023. CCL5-producing migratory
667 dendritic cells guide CCR5+ monocytes into the draining lymph nodes. *J. Exp. Med.* 220.
668 33. Engel, D. R., J. Maurer, A. P. Tittel, C. Weisheit, T. Cavlar, B. Schumak, A. Limmer, N.
669 van Rooijen, C. Trautwein, F. Tacke, and C. Kurts. 2008. CCR2 mediates homeostatic
670 and inflammatory release of Gr1(high) monocytes from the bone marrow, but is
671 dispensable for bladder infiltration in bacterial urinary tract infection. *J Immunol* 181:
672 5579-5586.
673 34. Serbina, N. V., and E. G. Pamer. 2006. Monocyte emigration from bone marrow during
674 bacterial infection requires signals mediated by chemokine receptor CCR2. *Nat.*
675 *Immunol.* 7: 311-317.
676 35. Larkin, B., V. Ilyukha, M. Sorokin, A. Buzdin, E. Vannier, and A. Poltorak. 2017.
677 Cutting Edge: Activation of STING in T Cells Induces Type I IFN Responses and Cell
678 Death. *J Immunol* 199: 397-402.
679 36. Zhou, T., W. Damsky, O. E. Weizman, M. K. McGeary, K. P. Hartmann, C. E. Rosen, S.
680 Fischer, R. Jackson, R. A. Flavell, J. Wang, M. F. Sanmamed, M. W. Bosenberg, and A.
681 M. Ring. 2020. IL-18BP is a secreted immune checkpoint and barrier to IL-18
682 immunotherapy. *Nature* 583: 609-614.

683 37. Hu, B., J. Ren, Y. Luo, B. Keith, R. M. Young, J. Scholler, Y. Zhao, and C. H. June.
684 2017. Augmentation of Antitumor Immunity by Human and Mouse CAR T Cells
685 Secreting IL-18. *Cell Rep* 20: 3025-3033.
686 38. DeNardo, D. G., and B. Ruffell. 2019. Macrophages as regulators of tumour immunity
687 and immunotherapy. *Nat Rev Immunol* 19: 369-382.
688 39. Abram, C. L., G. L. Roberge, Y. Hu, and C. A. Lowell. 2014. Comparative analysis of
689 the efficiency and specificity of myeloid-Cre deleting strains using ROSA-EYFP reporter
690 mice. *J Immunol Methods* 408: 89-100.
691 40. Lam, K. C., R. E. Araya, A. Huang, Q. Chen, M. Di Modica, R. R. Rodrigues, A. Lopes,
692 S. B. Johnson, B. Schwarz, E. Bohrnsen, A. P. Cogdill, C. M. Bosio, J. A. Wargo, M. P.
693 Lee, and R. S. Goldszmid. 2021. Microbiota triggers STING-type I IFN-dependent
694 monocyte reprogramming of the tumor microenvironment. *Cell* 184: 5338-5356 e5321.
695 41. Kwart, D., J. He, S. Srivatsan, C. Lett, J. Golubov, E. M. Oswald, P. Poon, X. Ye, J.
696 Waite, A. G. Zaretsky, S. Haxhinasto, E. Au-Yeung, N. T. Gupta, J. Chiu, C. Adler, S.
697 Cherravuru, E. Malahias, N. Negron, K. Lanza, A. Coppola, M. Ni, H. Song, Y. Wei, G.
698 S. Atwal, L. Macdonald, N. S. Oristian, W. Poueymirou, V. Jankovic, M. Fury, I. Lowy,
699 A. J. Murphy, M. A. Sleeman, B. Wang, and D. Skokos. 2022. Cancer cell-derived type I
700 interferons instruct tumor monocyte polarization. *Cell Reports* 41.
701 42. Alicea-Torres, K., E. Sanseviero, J. Gui, J. Chen, F. Veglia, Q. Yu, L. Donthireddy, A.
702 Kossenkov, C. Lin, S. Fu, C. Mulligan, B. Nam, G. Masters, F. Denstman, J. Bennett, N.
703 Hockstein, A. Rynda-Apple, Y. Nefedova, S. Y. Fuchs, and D. I. Gabrilovich. 2021.
704 Immune suppressive activity of myeloid-derived suppressor cells in cancer requires
705 inactivation of the type I interferon pathway. *Nat Commun* 12: 1717.

706 43. Kuhn, S., J. Yang, and F. Ronchese. 2015. Monocyte-Derived Dendritic Cells Are
707 Essential for CD8(+) T Cell Activation and Antitumor Responses After Local
708 Immunotherapy. *Front Immunol* 6: 584.
709 44. Tang-Huau, T. L., P. Gueguen, C. Goudot, M. Durand, M. Bohec, S. Baulande, B.
710 Pasquier, S. Amigorena, and E. Segura. 2018. Human in vivo-generated monocyte-
711 derived dendritic cells and macrophages cross-present antigens through a vacuolar
712 pathway. *Nat Commun* 9: 2570.
713 45. Faure, F., M. Jouve, I. Lebhar-Peguillet, C. Sadaka, F. Sepulveda, O. Lantz, S. Berre, R.
714 Gaudin, S. Sanchez-Ramon, and S. Amigorena. 2018. Blood monocytes sample
715 MelanA/MART1 antigen for long-lasting cross-presentation to CD8(+) T cells after
716 differentiation into dendritic cells. *Int J Cancer* 142: 133-144.
717 46. Duong, E., T. B. Fessenden, E. Lutz, T. Dinter, L. Yim, S. Blatt, A. Bhutkar, K. D.
718 Wittrup, and S. Spranger. 2021. Type I interferon activates MHC class I-dressed
719 CD11b(+) conventional dendritic cells to promote protective anti-tumor CD8(+) T cell
720 immunity. *Immunity*.
721 47. Leal, J. M., J. Y. Huang, K. Kohli, C. Stoltzfus, M. R. Lyons-Cohen, B. E. Olin, M. Gale,
722 Jr., and M. Y. Gerner. 2021. Innate cell microenvironments in lymph nodes shape the
723 generation of T cell responses during type I inflammation. *Sci Immunol* 6.
724 48. Jneid, B., A. Bochnakian, C. Hoffmann, F. Delisle, E. Djacoto, P. Sirven, J. Denizeau, C.
725 Sedlik, Y. Gerber-Ferder, F. Fiore, R. Akyol, C. Brousse, R. Kramer, I. Walters, S.
726 Carlioz, H. Salmon, B. Malissen, M. Dalod, E. Piaggio, and N. Manel. 2023. Selective
727 STING stimulation in dendritic cells primes antitumor T cell responses. *Sci Immunol* 8:
728 eabn6612.

729 49. Zhu, Q., and T. D. Kanneganti. 2017. Cutting Edge: Distinct Regulatory Mechanisms
730 Control Proinflammatory Cytokines IL-18 and IL-1beta. *J Immunol* 198: 4210-4215.
731 50. Ahn, J., S. Son, S. C. Oliveira, and G. N. Barber. 2017. STING-Dependent Signaling
732 Underlies IL-10 Controlled Inflammatory Colitis. *Cell Rep* 21: 3873-3884.
733 51. Wang, W., D. Hu, C. Wu, Y. Feng, A. Li, W. Liu, Y. Wang, K. Chen, M. Tian, F. Xiao,
734 Q. Zhang, M. A. Shereen, W. Chen, P. Pan, P. Wan, K. Wu, and J. Wu. 2020. STING
735 promotes NLRP3 localization in ER and facilitates NLRP3 deubiquitination to activate
736 the inflammasome upon HSV-1 infection. *PLoS Pathog* 16: e1008335.
737 52. Gaidt, M. M., T. S. Ebert, D. Chauhan, K. Ramshorn, F. Pinci, S. Zuber, F. O'Duill, J. L.
738 Schmid-Burgk, F. Hoss, R. Buhmann, G. Wittmann, E. Latz, M. Subklewe, and V.
739 Hornung. 2017. The DNA Inflammasome in Human Myeloid Cells Is Initiated by a
740 STING-Cell Death Program Upstream of NLRP3. *Cell* 171: 1110-1124 e1118.
741 53. Swanson, K. V., R. D. Junkins, C. J. Kurkjian, E. Holley-Guthrie, A. A. Pendse, R. El
742 Morabiti, A. Petrucelli, G. N. Barber, C. A. Benedict, and J. P. Ting. 2017. A
743 noncanonical function of cGAMP in inflammasome priming and activation. *J Exp Med*
744 214: 3611-3626.
745
746
747

748 **Footnotes**

749

750 1. **Funding:** This research was funded by Canadian Cancer Society grant #706759, Canadian
751 Institutes of Health Research (CIHR) grants # FDN-143250, PJ4-185649 and PJT 190128
752 (all to THW) and a CIHR Canada graduate scholarships doctoral award (MG). THW holds
753 the Canada research chair in anti-viral immunity at the University of Toronto

754 2. **Current address:** Department of Microbiology & Immunology, University of California,
755 San Francisco, San Francisco, California, USA.

756 3. **Corresponding author:** Corresponding author: Dr. Tania H. Watts, Department of
757 Immunology, University of Toronto, 1 King's College Circle, Toronto, ON M5S 1A8,
758 Canada. E-mail address: tania.watts@utoronto.ca Tel 416-978-4551

759

760

761 **Figures**

762 **Figure 1. InfMCs accumulate in tumors and show CCR5-dependent trafficking to LN**
763 **following STING agonist treatment. (A-H)** STING agonists drive the accumulation of $CD64^+$
764 $MAR\text{-}1^+$ infMCs in the LN and tumor. **(A)** Experimental layout for panels (B-H). Mice were
765 inoculated with 10^6 B16.OVA cells intradermally and given an intratumoral injection of ADU-
766 S100 or vehicle 12 days later. Tumors and draining LNs were harvested for flow cytometric
767 analysis at 0-5 days post-treatment. (**B)** Gating strategy for identification of cDC1
768 ($CD26^+MHCII^{hi}CD11c^+XCR1^+$), cDC2 ($CD26^+MHCII^{hi}CD11c^+CD172^+$), $Ly6C^{hi}$ MCs (CD26-
769 $CD11b^+Ly6G\text{-}Ly6C^+$) and infMCs ($CD26\text{-}CD11b^+Ly6G\text{-}Ly6C^+CD64^+MAR\text{-}1^+$) in the LN and
770 tumor, starting from single, live $CD45^+$ cells. **(C-H)** Number and percentage of cells in the LN (C-
771 E) and tumor (F-H) at indicated time points after treatment with ADU-S100 or vehicle. **(I-K)**
772 InfMCs carry tumor antigens to the LN. **(I)** Experimental layout for panels (J,K). C57BL/6 mice
773 were inoculated with 10^6 B16.OVA.tomato cells intradermally and given ADU-S100 or vehicle 12
774 days later. LNs were collected for flow cytometry on day 2 post-treatment. **(J)** Representative flow
775 plots. **(D)** Tomato signal in LN APC populations depicted as the tomato MFI (left panel), %
776 $tomato^+$ (middle panel) and absolute number of $tomato^+$ cells (right panel). (L) Experimental
777 design for panels (M-N). B16.OVA.tomato tumor-bearing C57BL/6 mice were given 10mg/kg
778 maraviroc or PBS treatment 4 hours prior to ADU-S100 or vehicle treatment. TDLNs were
779 collected for flow cytometry on day 1 post-treatment. (M) Tomato signal in LN $Ly6C^{hi}$ MC
780 population depicted as absolute number of $tomato^+$ cells. (N) CCR5 expression on $Ly6C^{hi}$ MCs,
781 cDC1 and cDC2 in TDLN one day after ADU-S100 treatment. Data are pooled from two or three
782 independent experiments, each with 3-6 mice per group. Unpaired t-test (D,E,G,H), two-way
783 ANOVA (K,M), or one-way ANOVA with Sidak's multiple comparisons test (N) was performed.

784

785

786 **Figure 2. InfMCs are required for optimal responses to STING agonist therapy. (A)** Number
787 and percentage of infMCs in B16.OVA tumors of *Ccr2*$^{+/+}$ and *Ccr2*$^{-/-}$ mice two days post-treatment
788 with ADU-S100 or vehicle. **(B-C),** Volume of B16.OVA intradermal tumors (B) or MC-38
789 subcutaneous tumors (C) in *Ccr2*$^{+/+}$ and *Ccr2*$^{-/-}$ mice treated with ADU-S100 or vehicle on days
790 indicated by an arrow. **(D-E),** Ki-67 staining on LN H-2K^{b} SIINFEKL tetramer^{+} CD8^{+} T cells (D)
791 or NK cells (E) three days post-treatment with ADU-S100 or vehicle. Data are representative of
792 two independent experiments. One-way ANOVA (A, D-E), or two-way ANOVA with Sidak's
793 multiple comparisons test (B,C) was performed.

794

795 **Figure 3. Intrinsic IFN-I signaling drives an inflammatory phenotype in Ly6C^{hi} MCs but is**
796 **dispensable for their migration to the LN. (A)** Experimental layout for panels (B,C). *Ifnar1*$^{fl/fl}$
797 and *Ifnar1*$^{fl/fl}$ *Lyz2-Cre* mice were inoculated with B16.OVA tumors and treated with ADU-S100
798 or vehicle 12 days later. **(B)** IFNAR1, CD64 and MAR-1 staining on Ly6C^{hi} MCs from the
799 B16F10.OVA tumors of *Ifnar1*$^{fl/fl}$ and *Ifnar1*$^{fl/fl}$ *Lyz2-Cre* mice on day 5 post-treatment. **(C)**
800 Volume of B16F10.OVA tumors in *Ifnar1*$^{fl/fl}$ and *Ifnar1*$^{fl/fl}$ *Lyz2-Cre* mice treated with ADU-S100
801 on day 11. **(D)** Experimental layout for panels (E-G). Irradiated CD45.1/.2 mice were reconstituted
802 with a 1:1 mixture of CD45.1 *Ifnar1*$^{+/+}$ and CD45.2 *Ifnar1*$^{-/-}$ bone marrow cells. After >90 days
803 reconstitution, mice were inoculated with 10^{6} B16F10.OVA cells intradermally and given ADU-
804 S100 or vehicle intratumorally 12 days later. TDLNs and tumors were collected 1- and 2-days
805 post-treatment, respectively for flow cytometric analysis. **(E)** Absolute numbers of *Ifnar1*$^{+/+}$ and
806 *Ifnar1*$^{-/-}$ cDC1, cDC2 and Ly6C^{hi} MCs in the TDLNs (top) and tumors (bottom) of the mixed bone

807 marrow chimeric mice. **(F)** Percentage of Ly6C^{hi} MCs that express the infMC markers CD64 and
808 MAR-1 in the TDLNs (top) and tumors (bottom) of the mixed bone marrow chimeric mice. **(G)**
809 Mean fluorescent intensity of CD64 and MAR-1 on Ly6C^{hi} MCs in the TDLNs (top) and tumors
810 (bottom) of the mixed bone marrow chimeric mice. Data are pooled from two independent
811 experiments with 3-4 mice each.Unpaired t-test (B), two-way ANOVA with Sidak's multiple
812 comparisons test (C), or One-way ANOVA with Tukey's multiple comparisons test (E-G) was
813 performed.
814
815
816 **Figure 4. Intrinsic IFN-I signaling drives an inflammatory transcriptional state in LN and**
817 **tumor monocytes.** CITE-sequencing analysis of myeloid cells from the LNs and tumors of *Ifnar1*
818 mixed bone marrow chimeric mice on days 1 and 2 post-treatment with ADU-S100 or vehicle. **(A)**
819 Experimental design. **(B-C)** UMAP of cDC, monocyte and macrophage populations in the LN. (B)
820 and tumor (C). **(D)** Proportion of cells in each cluster derived from each genotype and treatment
821 condition. **(E-F)** UMAP depicting the IFN-I signature score for each cell in the LN (E) and tumor
822 (F). On the right, dotplots depicting the expression of common ISGs across clusters. **(G)**
823 Percentage of total monocytes/macrophages in each group derived from each cluster. **(H)**
824 Heatmaps depicting top DEGs across or tumor monocyte/macrophage clusters. **(I)** Pathway
825 enrichment analysis (g:Profiler, GO biological processes) using DEGs for each tumor
826 monocyte/macrophage cluster (Mono/Mac 1-5). **(J)** Expression of genes involved in antigen
827 processing and presentation via MHC class I in monocyte/macrophages from the LN and tumor of
828 *Ifnar1* mixed bone marrow chimeric mice treated with ADU-S100 or vehicle.
829

830 **Figure 5. InfMCs have a unique inflammatory program compared to infDCs. (A)**
831 Inflammatory signatures for infMCs, infDC1 and infDC2 were calculated and compared in a Venn
832 diagram. **(B)** Heatmaps depicting differential expression of selected inflammatory genes across
833 infAPC populations. **(C)** Heatmap depicting the percentage of cells in each infAPC population in
834 which the indicated regulons are active, as determined by single-cell regulatory network inference
835 analysis.
836
837 **Figure 6. IL-18 is required for optimal tumor control in response to STING agonists. (A)**
838 NicheNet analysis of receptor ligand interactions between infAPC populations and $CD8^+$ T cells
839 or NK cells. **(B)** Gating strategy to identify H-$2K^b$ SIINFEKL $tetramer^+$ $CD8^+$ T cells and NK cells
840 in the LNs starting from live $CD45^+$ cells. **(C-D)** Mice were administered 200 µg anti-IL-18 or
841 IgG2a intraperitoneally twice: one day before and one day after intra-tumoral administration of
842 ADU-S100 or vehicle control. **(C)** Expression of IL-18R1 on LN H-$2K^b$ SIINFEKL $tetramer^+$
843 $CD8^+$ T cells and NK cells 3 days post-treatment with ADU-S100. **(D)** Volume of B16.OVA
844 tumors in mice treated with anti-IL-18 or IgG2a and ADU-S100. (**E**) Volume of B16.OVA tumors
845 in *Ccr2*$^{+/+}$ and *Ccr2*$^{-/-}$ littermate mice treated with anti-IL-18 or IgG2a and ADU-S100. Data are
846 representative of two independent experiments, each with 4-5 mice per group. One-way ANOVA
847 (C) or Two-way ANOVA with Sidak's multiple comparisons test (D-E) was performed.
848
849
850
851
852

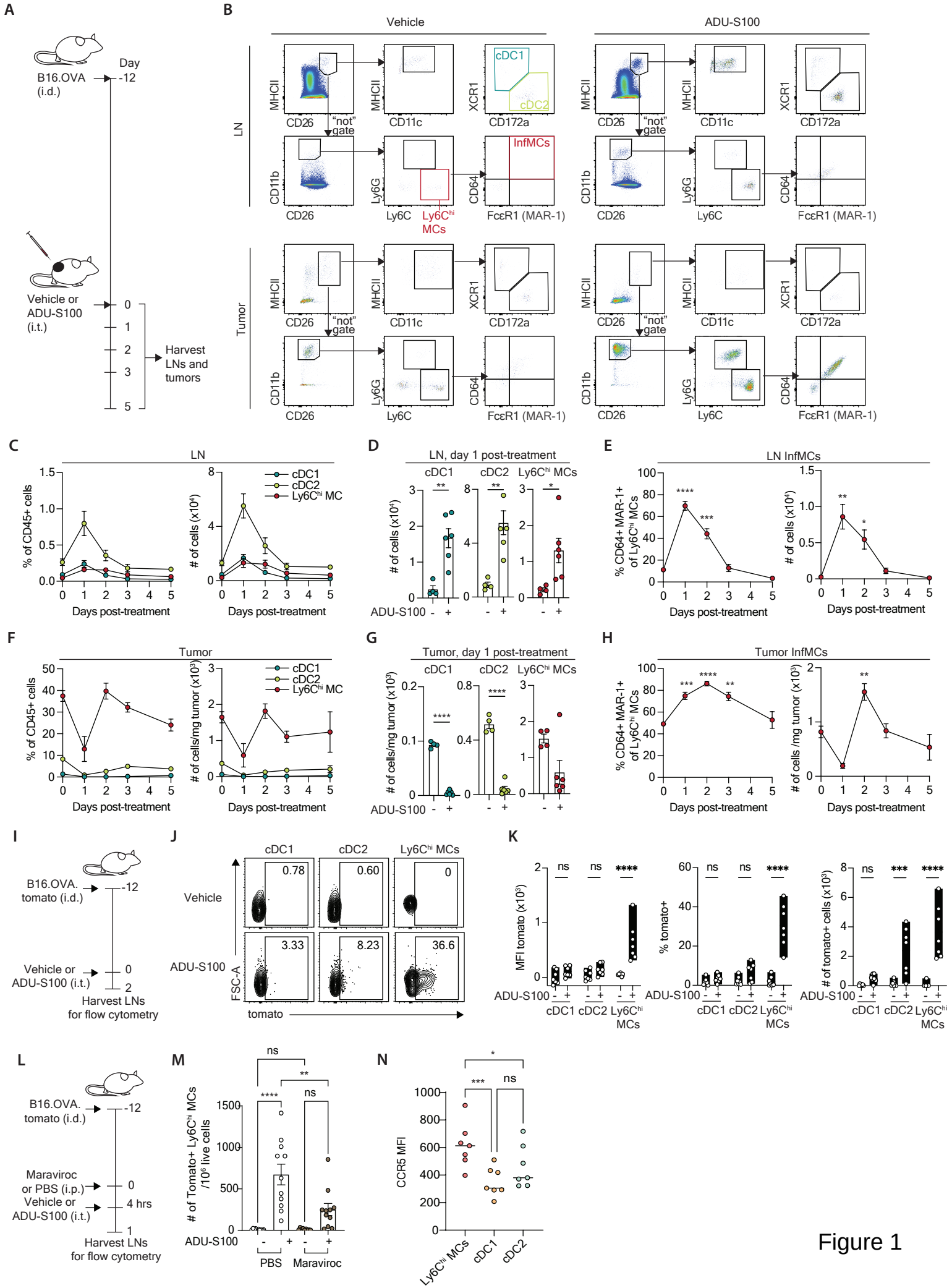
A
B16.OVA (i.d.)
Day -12
Vehicle or ADU-S100 (i.t.)
0
1
2
3
5
Harvest LNs and tumors
B
Vehicle
ADU-S100
LN
Tumor
MHCII
CD26
"not" gate
CD11c
XCR1
CD172a
cDC1
cDC2
CD11b
Ly6G
Ly6C
CD64
FcεR1 (MAR-1)
InfMCs
Ly6C^hi MCs
C
LN
% of CD45+ cells
# of cells (x10^4)
cDC1
cDC2
Ly6C^hi MC
Days post-treatment
D
LN, day 1 post-treatment
cDC1
cDC2
Ly6C^hi MCs
# of cells (x10^4)
ADU-S100
E
LN InfMCs
% CD64+ MAR-1+ of Ly6C^hi MCs
# of cells (x10^4)
F
Tumor
% of CD45+ cells
# of cells/mg tumor (x10^3)
G
Tumor, day 1 post-treatment
H
Tumor InfMCs
I
B16.OVA. tomato (i.d.)
Vehicle or ADU-S100 (i.t.)
Harvest LNs for flow cytometry
J
Vehicle
ADU-S100
FSC-A
tomato
0.78
0.60
0
3.33
8.23
36.6
K
MFI tomato (x10^3)
% tomato+
# of tomato+ cells (x10^3)
ns
****
***
L
B16.OVA. tomato (i.d.)
Maraviroc or PBS (i.p.)
Vehicle or ADU-S100 (i.t.)
4 hrs
Harvest LNs for flow cytometry
M
# of Tomato+ Ly6C^hi MCs /10^6 live cells
PBS
Maraviroc
N
CCR5 MFI
Ly6C^hi MCs
cDC1
cDC2

Figure 1

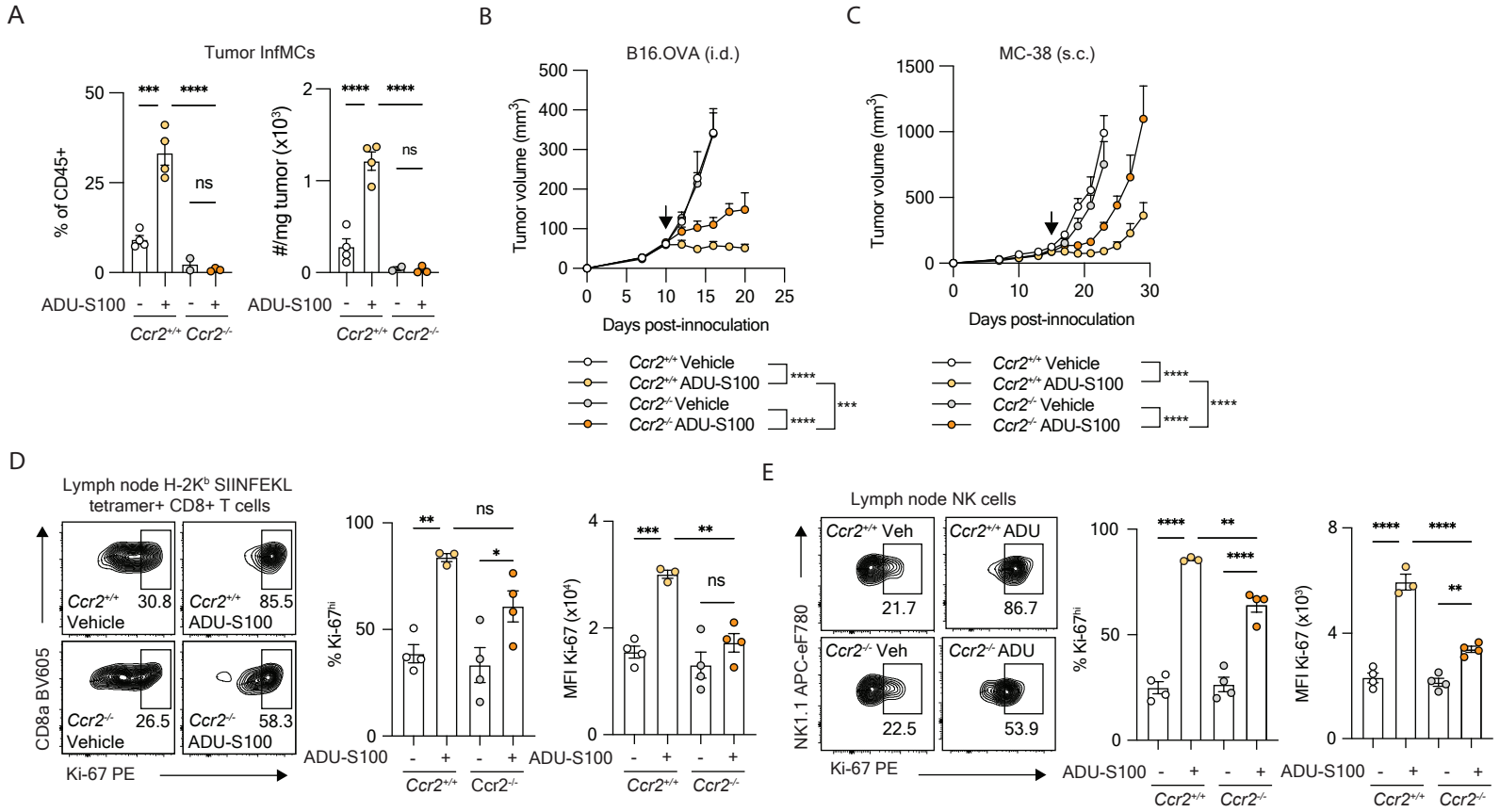
A
Tumor InfMCs
% of CD45+
#/mg tumor (x10³)
ADU-S100
Ccr2+/+ Ccr2-/-
B
B16.OVA (i.d.)
Tumor volume (mm³)
Days post-innoculation
Ccr2+/+ Vehicle
Ccr2+/+ ADU-S100
Ccr2-/- Vehicle
Ccr2-/- ADU-S100
C
MC-38 (s.c.)
D
Lymph node H-2Kᵇ SIINFEKL tetramer+ CD8+ T cells
CD8a BV605
Ki-67 PE
30.8
85.5
26.5
58.3
% Ki-67hi
MFI Ki-67 (x10⁴)
E
Lymph node NK cells
NK1.1 APC-eF780
21.7
86.7
22.5
53.9
MFI Ki-67 (x10³)

Figure 2

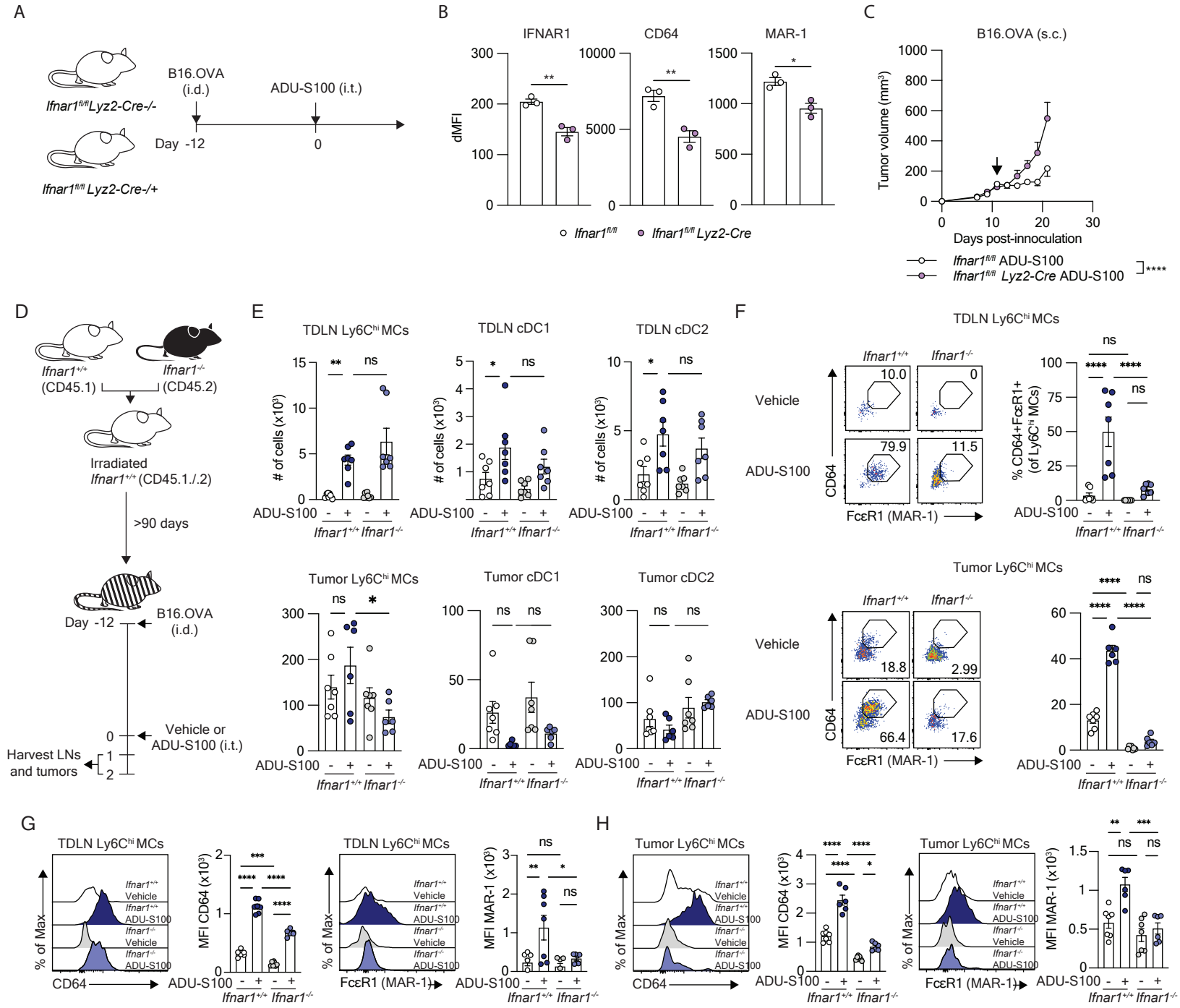
A
Ifnar1fl/flLyz2-Cre-/-
Ifnar1fl/fl Lyz2-Cre-/+
B16.OVA (i.d.)
ADU-S100 (i.t.)
Day -12
0
B
IFNAR1
CD64
MAR-1
dMFI
Ifnar1fl/fl
Ifnar1fl/fl Lyz2-Cre
C
B16.OVA (s.c.)
Tumor volume (mm3)
Days post-innoculation
Ifnar1fl/fl ADU-S100
Ifnar1fl/fl Lyz2-Cre ADU-S100
D
Ifnar1+/+ (CD45.1)
Ifnar1-/- (CD45.2)
Irradiated Ifnar1+/+ (CD45.1./.2)
>90 days
Day -12
B16.OVA (i.d.)
Vehicle or ADU-S100 (i.t.)
Harvest LNs and tumors
E
TDLN Ly6Chi MCs
TDLN cDC1
TDLN cDC2
# of cells (x103)
ADU-S100
Ifnar1+/+ Ifnar1-/-
Tumor Ly6Chi MCs
Tumor cDC1
Tumor cDC2
F
TDLN Ly6Chi MCs
Vehicle
ADU-S100
CD64
FcεR1 (MAR-1)
% CD64+FcεR1+ (of Ly6Chi MCs)
Tumor Ly6Chi MCs
G
TDLN Ly6Chi MCs
% of Max
CD64
MFI CD64 (x103)
FcεR1 (MAR-1)
MFI MAR-1 (x103)
H
Tumor Ly6Chi MCs

Figure 3

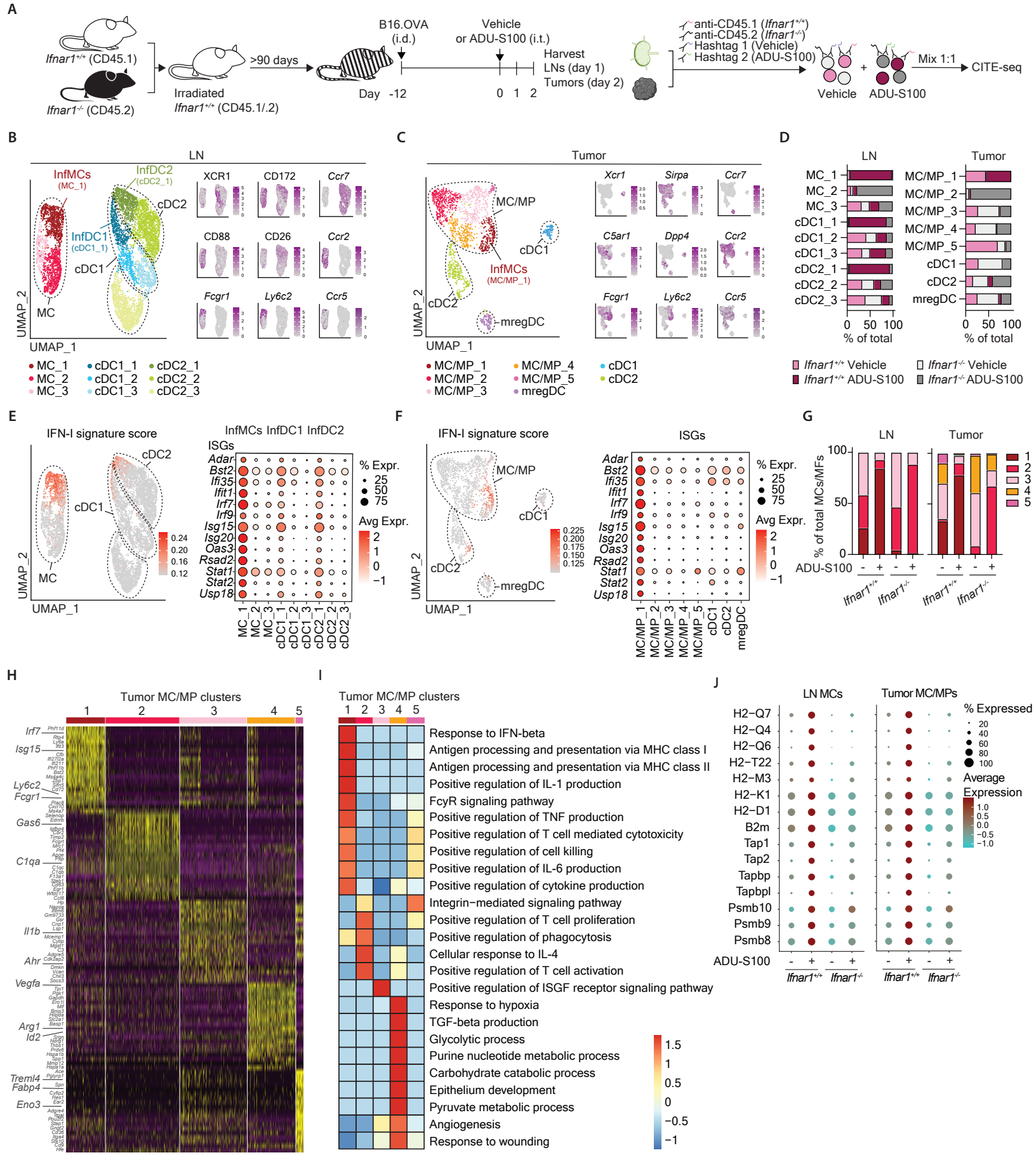
A
Ifnar1+/+ (CD45.1)
Ifnar1-/- (CD45.2)
Irradiated Ifnar1+/+ (CD45.1/.2)
>90 days
B16.OVA (i.d.)
Vehicle or ADU-S100 (i.t.)
Day -12
0 1 2
Harvest
LNs (day 1)
Tumors (day 2)
anti-CD45.1 (Ifnar1+/+)
anti-CD45.2 (Ifnar1-/-)
Hashtag 1 (Vehicle)
Hashtag 2 (ADU-S100)
Vehicle
ADU-S100
Mix 1:1
CITE-seq
B
LN
InfMCs (MC_1)
InfDC2 (cDC2_1)
cDC2
InfDC1 (cDC1_1)
cDC1
MC
UMAP_1
UMAP_2
XCR1
CD172
Ccr7
CD88
CD26
Ccr2
Fcgr1
Ly6c2
Ccr5
MC_1
MC_2
MC_3
cDC1_1
cDC1_2
cDC1_3
cDC2_1
cDC2_2
cDC2_3
C
Tumor
MC/MP
cDC1
InfMCs (MC/MP_1)
cDC2
mregDC
Xcr1
Sirpa
Ccr7
C5ar1
Dpp4
Ccr2
Fcgr1
Ly6c2
Ccr5
MC/MP_1
MC/MP_2
MC/MP_3
MC/MP_4
MC/MP_5
mregDC
cDC1
cDC2
D
LN
Tumor
% of total
Ifnar1+/+ Vehicle
Ifnar1+/+ ADU-S100
Ifnar1-/- Vehicle
Ifnar1-/- ADU-S100
E
IFN-I signature score
ISGs
InfMCs InfDC1 InfDC2
Adar
Bst2
Ifi35
Ifit1
Irf7
Irf9
Isg15
Isg20
Oas3
Rsad2
Stat1
Stat2
Usp18
% Expr.
Avg Expr.
F
IFN-I signature score
ISGs
G
LN
Tumor
% of total MCs/MFs
ADU-S100
Ifnar1+/+
Ifnar1-/-
H
Tumor MC/MP clusters
Irf7
Isg15
Ly6c2
Fcgr1
Gas6
C1qa
Il1b
Ahr
Vegfa
Arg1
Id2
Tremlin4
Fabp4
Eno3
I
Tumor MC/MP clusters
Response to IFN-beta
Antigen processing and presentation via MHC class I
Antigen processing and presentation via MHC class II
Positive regulation of IL-1 production
FcγR signaling pathway
Positive regulation of TNF production
Positive regulation of T cell mediated cytotoxicity
Positive regulation of cell killing
Positive regulation of IL-6 production
Positive regulation of cytokine production
Integrin-mediated signaling pathway
Positive regulation of T cell proliferation
Positive regulation of phagocytosis
Cellular response to IL-4
Positive regulation of T cell activation
Positive regulation of ISGF receptor signaling pathway
Response to hypoxia
TGF-beta production
Glycolytic process
Purine nucleotide metabolic process
Carbohydrate catabolic process
Epithelium development
Pyruvate metabolic process
Angiogenesis
Response to wounding
J
LN MCs
Tumor MC/MPs
H2-Q7
H2-Q4
H2-Q6
H2-T22
H2-M3
H2-K1
H2-D1
B2m
Tap1
Tap2
Tapbp
Tapbpl
Psmb10
Psmb9
Psmb8
% Expressed
Average Expression

Figure 4

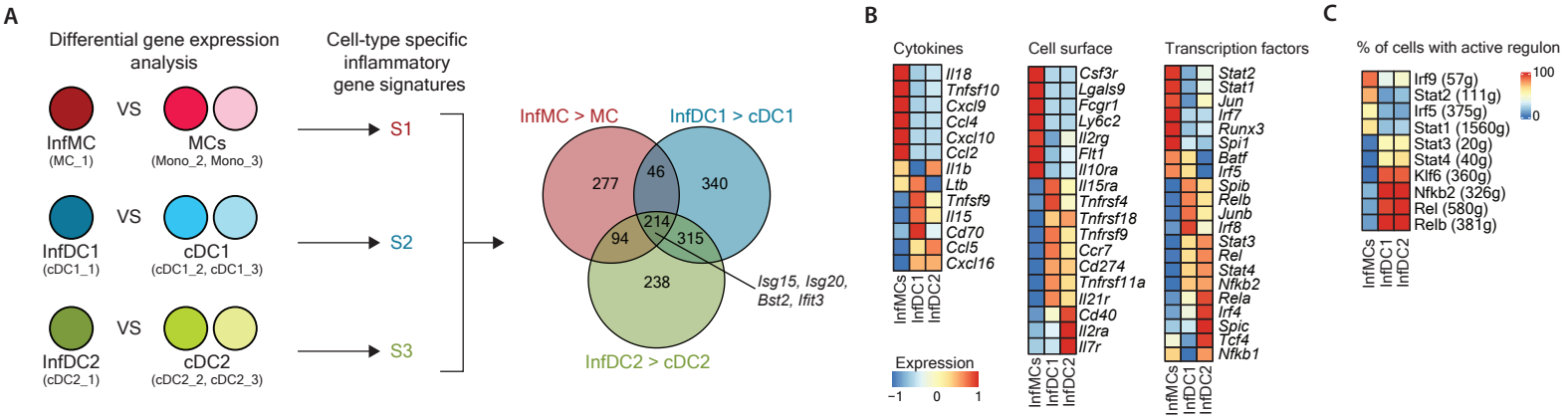
A
Differential gene expression analysis
Cell-type specific inflammatory gene signatures
InfMC
(MC_1)
VS
MCs
(Mono_2, Mono_3)
S1
InfDC1
(cDC1_1)
VS
cDC1
(cDC1_2, cDC1_3)
S2
InfDC2
(cDC2_1)
VS
cDC2
(cDC2_2, cDC2_3)
S3
InfMC > MC
InfDC1 > cDC1
InfDC2 > cDC2
277
46
340
214
94
315
238
Isg15, Isg20, Bst2, Ifit3
B
Cytokines
Il18
Tnfsf10
Cxcl9
Ccl4
Cxcl10
Ccl2
Il1b
Ltb
Tnfsf9
Il15
Cd70
Ccl5
Cxcl16
InfMCs
InfDC1
InfDC2
Expression
−1
0
1
Cell surface
Csf3r
Lgals9
Fcgr1
Ly6c2
Il2rg
Flt1
Il10ra
Il15ra
Tnfrsf4
Tnfrsf18
Tnfrsf9
Ccr7
Cd274
Tnfrsf11a
Il21r
Cd40
Il2ra
Il7r
InfMCs
InfDC1
InfDC2
Transcription factors
Stat2
Stat1
Jun
Irf7
Runx3
Spi1
Batf
Irf5
Spib
Relb
Junb
Irf8
Stat3
Rel
Stat4
Nfkb2
Rela
Irf4
Spic
Tcf4
Nfkb1
InfMCs
InfDC1
InfDC2
C
% of cells with active regulon
Irf9 (57g)
Stat2 (111g)
Irf5 (375g)
Stat1 (1560g)
Stat3 (20g)
Stat4 (40g)
Klf6 (360g)
Nfkb2 (326g)
Rel (580g)
Relb (381g)
100
0
InfMCs
InfDC1
InfDC2

Figure 5

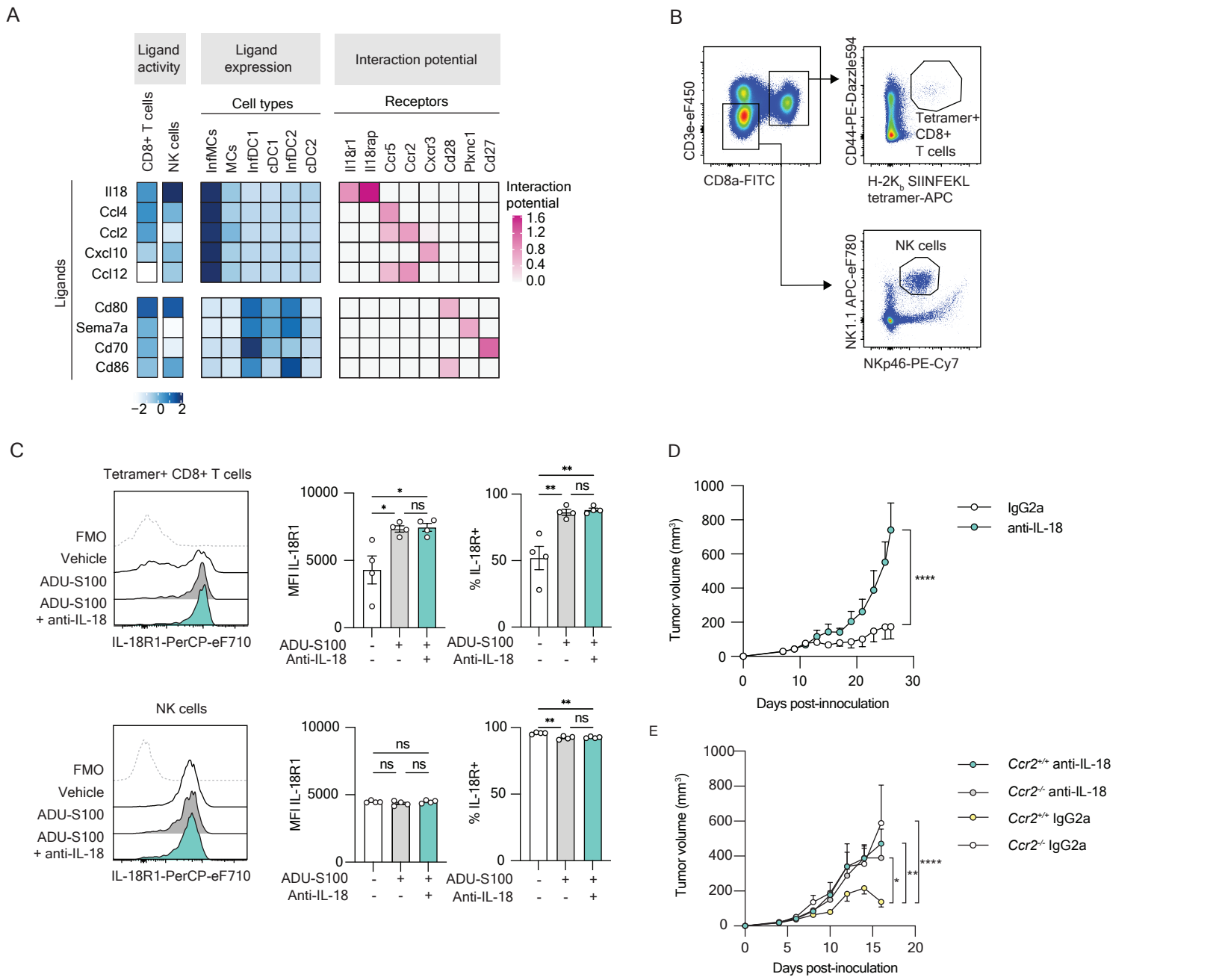
A
Ligand activity
Ligand expression
Interaction potential
CD8+ T cells
NK cells
Cell types
Receptors
InfMCs
MCs
InfDC1
cDC1
InfDC2
cDC2
Il18r1
Il18rap
Ccr5
Ccr2
Cxcr3
Cd28
Plxnc1
Cd27
Ligands
Il18
Ccl4
Ccl2
Cxcl10
Ccl12
Cd80
Sema7a
Cd70
Cd86
Interaction potential
1.6
1.2
0.8
0.4
0.0
−2 0 2
B
CD3e-eF450
CD8a-FITC
CD44-PE-Dazzle594
H-2Kb SIINFEKL tetramer-APC
Tetramer+ CD8+ T cells
NK cells
NK1.1 APC-eF780
NKp46-PE-Cy7
C
Tetramer+ CD8+ T cells
FMO
Vehicle
ADU-S100
ADU-S100 + anti-IL-18
IL-18R1-PerCP-eF710
MFI IL-18R1
% IL-18R+
ADU-S100
Anti-IL-18
NK cells
D
Tumor volume (mm³)
Days post-innoculation
IgG2a
anti-IL-18
E
Ccr2+/+ anti-IL-18
Ccr2-/- anti-IL-18
Ccr2+/+ IgG2a
Ccr2-/- IgG2a

Figure 6